

# Learning-associated astrocyte ensembles regulate memory recall

<https://doi.org/10.1038/s41586-024-08170-w>

Received: 27 December 2023

Accepted: 8 October 2024

Published online: 6 November 2024

 Check for updates

Michael R. Williamson<sup>1,2,3,6</sup>, Wookbong Kwon<sup>1,2,3,6</sup>, Junsung Woo<sup>1,2,3</sup>, Yeunjung Ko<sup>1,2,4</sup>, Ehsan Maleki<sup>1,2</sup>, Kwanha Yu<sup>1,2,3</sup>, Sanjana Murali<sup>1,2,5</sup>, Debosmita Sardar<sup>1,2,3</sup> & Benjamin Deneen<sup>1,2,3,4,5</sup>✉

The physical manifestations of memory formation and recall are fundamental questions that remain unresolved<sup>1</sup>. At the cellular level, ensembles of neurons called engrams are activated by learning events and control memory recall<sup>1–5</sup>. Astrocytes are found in close proximity to neurons and engage in a range of activities that support neurotransmission and circuit plasticity<sup>6–10</sup>. Moreover, astrocytes exhibit experience-dependent plasticity<sup>11–13</sup>, although whether specific ensembles of astrocytes participate in memory recall remains obscure. Here we show that learning events induce c-Fos expression in a subset of hippocampal astrocytes, and that this subsequently regulates the function of the hippocampal circuit in mice. Intersectional labelling of astrocyte ensembles with c-Fos after learning events shows that they are closely affiliated with engram neurons, and reactivation of these astrocyte ensembles stimulates memory recall. At the molecular level, learning-associated astrocyte (LAA) ensembles exhibit elevated expression of nuclear factor I-A, and its selective deletion from this population suppresses memory recall. Taken together, our data identify LAA ensembles as a form of plasticity that is sufficient to provoke memory recall and indicate that astrocytes are an active component of the engram.

Ensembles of neurons activated during a learning event that are both necessary and sufficient for subsequent memory recall form the cellular basis of memory and are referred to as engrams<sup>2–5</sup>. A hallmark feature of engram neurons is the induction of immediate early genes (IEGs), which mediate synaptic plasticity and are a crucial aspect of memory formation<sup>14,15</sup>. Accordingly, IEG-based tools have been used to tag and manipulate engram neurons, and the memories they represent, across a variety of brain regions<sup>2–5,16</sup>. Astrocytes are closely affiliated with neurons and, as part of the tripartite synapse, have essential roles in regulating circuit function, including those circuits associated with learning and memory<sup>9,17–20</sup>. Moreover, astrocytes exhibit experience-dependent plasticity, in which their activation states, transcriptional responses and functional properties are tuned to environmental stimuli and internal states<sup>11,12,21,22</sup>. Astrocytes are found in close proximity to neurons, respond to a range of experiential modalities and regulate learning behaviours, raising the possibility that they actively participate in memory formation and retrieval in coordination with neuronal ensembles. However, whether subsets of astrocytes respond to memory-inducing stimuli and form durable ensembles that are necessary and sufficient for memory storage and recall has remained unknown.

## Learning-dependent astrocyte activation

The function of hippocampal circuits and the memory-related behaviours they support depends on interactions with astrocytes<sup>23–25</sup>.

We previously found that astrocytes in the olfactory bulb undergo transcriptional and functional changes in response to neuronal activity to facilitate the processing of odour<sup>11</sup>. To examine how hippocampal astrocytes respond to neuronal activity, we chemogenetically activated neurons in the dentate gyrus by microinjecting adeno-associated virus (AAV)-hSyn-hM3D-mCherry into the dentate gyrus and, several weeks later, injecting mice with the hM3D agonist clozapine N-oxide (CNO, 0.3 mg per kg). This stimulation induced expression of the IEG c-Fos in a subset of astrocytes in both the dentate gyrus and CA1 (Extended Data Fig. 1a–d). We also found that selectively activating excitatory neurons in the dentate gyrus using AAV-CaMKII-hM3D-mCherry induced c-Fos expression in astrocytes (Extended Data Fig. 1e–g). Induction of astrocytic c-Fos following neuronal activation was preserved when inputs to the hippocampus were silenced using retrograde AAV-hSyn-hM4D-mCherry, indicating that the activity of local excitatory neurons is sufficient to drive c-Fos expression in astrocytes (Extended Data Fig. 1e,f). Next, we used a contextual fear-conditioning model to elicit natural activity in the hippocampal circuit and similarly found an activity-dependent increase in c-Fos-expressing astrocytes in CA1 and the dentate gyrus that peaked 1.5 h after the learning event (Fig. 1a–d). These findings indicate that hippocampal neuronal activity activates a subset of astrocytes.

Neuronal expression of c-Fos is activity dependent and is critical for synaptic plasticity and memory-dependent behaviours<sup>14,15,26</sup>, but the role of astrocytic c-Fos has not been studied in this context. To examine

<sup>1</sup>Center for Cell and Gene Therapy, Baylor College of Medicine, Houston, TX, USA. <sup>2</sup>Center for Cancer Neuroscience, Baylor College of Medicine, Houston, TX, USA. <sup>3</sup>Department of Neurosurgery, Baylor College of Medicine, Houston, TX, USA. <sup>4</sup>Program in Immunology and Microbiology, Baylor College of Medicine, Houston, TX, USA. <sup>5</sup>Program in Cancer Cell Biology, Baylor College of Medicine, Houston, TX, USA. <sup>6</sup>These authors contributed equally: Michael R. Williamson, Wookbong Kwon. ✉e-mail: deneen@bcm.edu

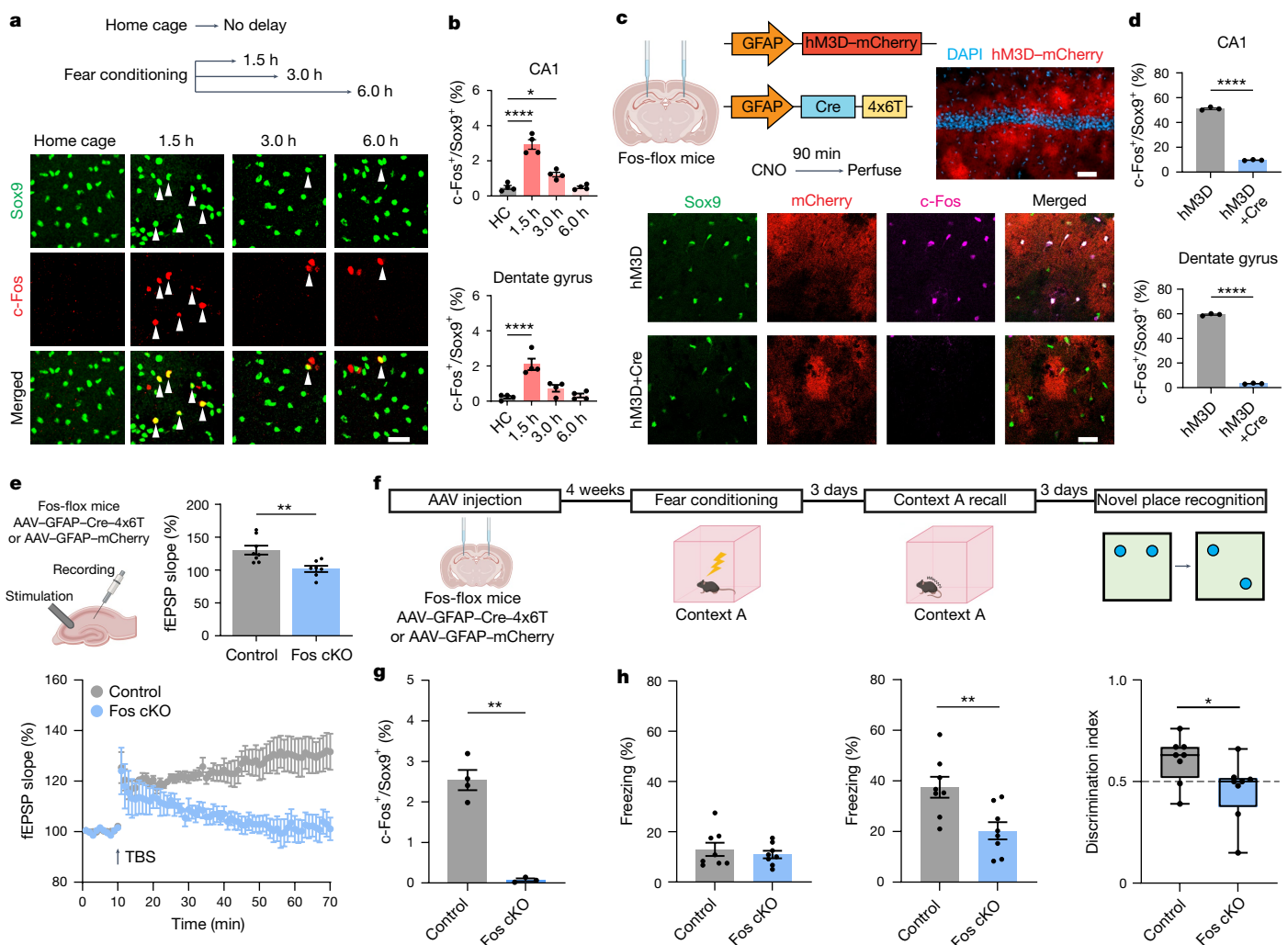


**Fig. 1 | Experience-dependent induction of astrocytic c-Fos regulates memory.** **a**, Experimental timeline and representative immunostaining of c-Fos expression in a subset of hippocampal astrocytes after fear learning. Arrowheads denote c-Fos<sup>+</sup>Sox9<sup>+</sup> cells. Scale bar, 30 μm. **b**, Quantification of c-Fos<sup>+</sup> astrocytes in area CA1 and the dentate gyrus after fear conditioning ( $n = 4$  mice per group; one-way analysis of variance (ANOVA) and Dunnett's post-hoc tests,  $*P = 0.0230$ ,  $****P < 0.0001$ ). HC, home cage. **c**, Schematics of AAV constructs, timeline and representative images for stimulating Gq-coupled signalling in astrocytes in control (hM3D) and Fos cKO (hM3D+Cre) mice. Scale bars: top, 50 μm; bottom, 30 μm. **d**, Quantification of c-Fos<sup>+</sup> astrocytes after CNO injection in hM3D and hM3D+Cre (Fos cKO) mice ( $n = 3$  mice per group; two-tailed t-test,  $****P < 0.0001$ ). **e**, Schematic and LTP traces in control (GFAP-mCherry) and Fos cKO (GFAP-Cre-4x6T) mice. Top right, mean field excitatory

postsynaptic potential (fEPSP) from the last 5 min of recordings ( $n = 8$  control,  $n = 7$  Fos cKO; two-tailed t-test,  $**P = 0.005$ ). TBS, theta burst stimulation. **f**, Timeline of the behavioural experiment comparing control and Fos cKO mice. **g**, Quantification of c-Fos expression in hippocampal astrocytes from control (GFAP-mCherry) and Fos cKO mice ( $n = 4$  control,  $n = 3$  Fos cKO; Welch's t-test,  $**P = 0.002$ ). **h**, Left, freezing behaviour in context A in the 2 min before foot shocks ( $n = 8$  mice per group; two-tailed t-test,  $P = 0.503$ ). Middle, freezing behaviour in the recall test in context A ( $n = 8$  mice per group; two-tailed t-test,  $**P = 0.006$ ). Right, place discrimination in the novel place recognition task ( $n = 8$  mice per group; two-tailed t-test,  $*P = 0.046$ ; horizontal line indicates median, box indicates quartiles and whiskers indicate minimum and maximum values). Data are mean  $\pm$  s.e.m. unless stated otherwise. Parts **c**, **e** and **f** were created using Biorender.com.

how experience-dependent c-Fos induction in astrocytes influences circuit plasticity in the hippocampus, we selectively knocked out Fos in hippocampal astrocytes using Fos-flox mice microinjected with glial fibrillary acid protein (GFAP)-Cre-4x6T AAVs, which contain a micro-RNA targeting cassette to eliminate off-target transgene expression in neurons<sup>27</sup> (Extended Data Fig. 2). We confirmed the efficiency of this knockout strategy by artificially inducing astrocytic c-Fos expression by chemogenetic activation of the Gq pathway in astrocytes<sup>24</sup> (Fig. 1c,d), and confirmed that there was Cre expression in all hippocampal sub-fields (Extended Data Fig. 3). Astrocyte-specific Fos conditional deletion (Fos cKO) diminished long-term potentiation (LTP) in hippocampal slices, indicating that astrocyte activation is essential for synaptic plasticity and learning-dependent behaviours (Fig. 1e). Accordingly, Fos cKO mice also exhibited impaired performance in contextual fear

conditioning and novel place recognition tasks (Fig. 1f–h and Extended Data Fig. 3). These behavioural deficits were coupled with mild reductions in astrocytic microdomain calcium activity and spontaneous neuronal activity in Fos cKO mice (Extended Data Fig. 4). Together, these findings demonstrate that activation of a subset of hippocampal astrocytes during learning is essential for circuit plasticity and memory recall.

## LAA ensembles

Our findings indicate that only a subset of astrocytes express c-Fos in response to hippocampal neuronal activity. These observations led us to deduce that an ensemble of astrocytes may selectively participate in the consolidation, storage and retrieval of the memory associated with

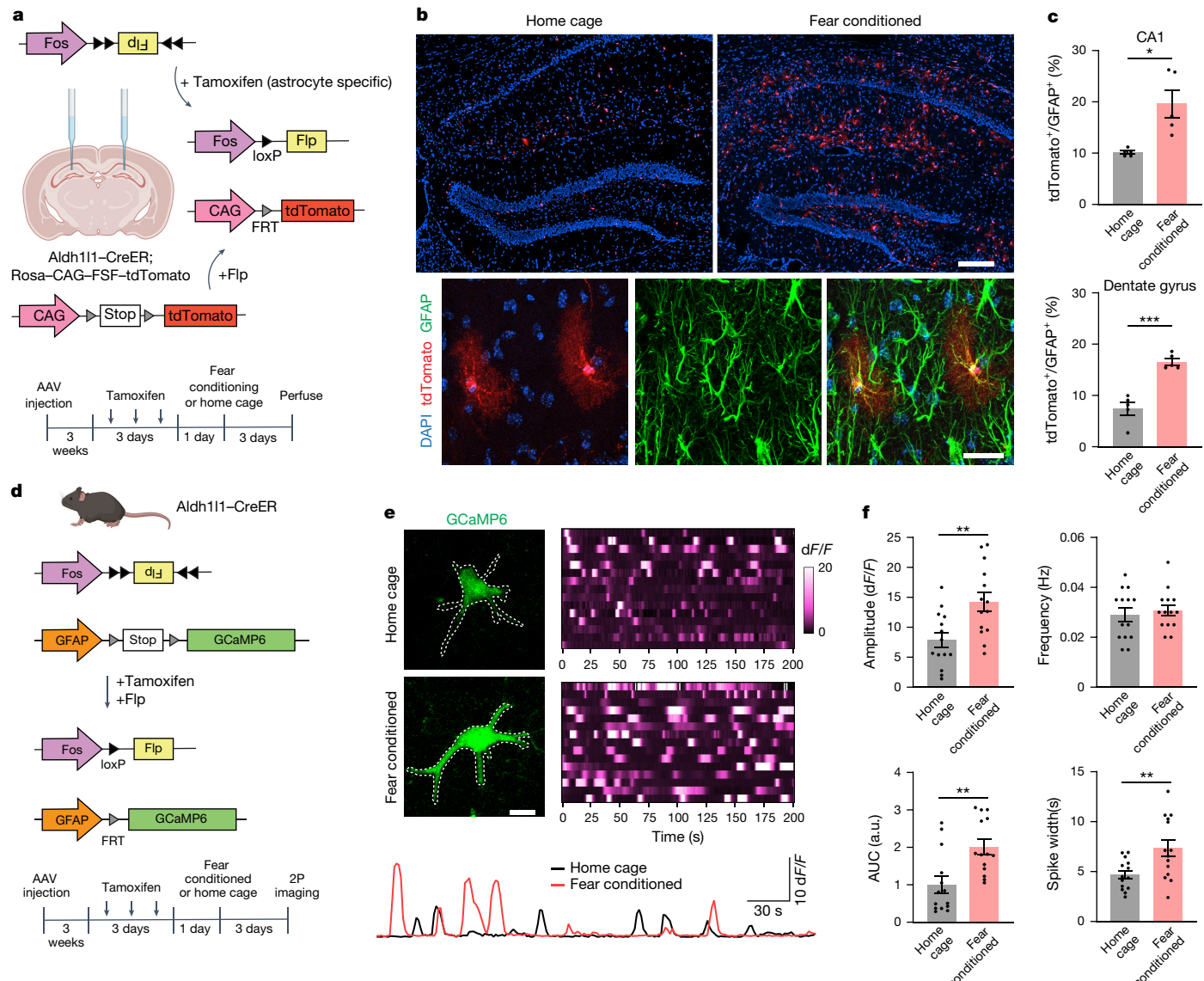


**Fig. 2 | Genetic access to LAA ensembles.** **a**, Schematic of the genetic system and timeline for labelling LAAs using AAV-Fos-Flex-Flp in Aldh1l1-CreER;Rosa-CAG-FSF-tdTomato mice. **b**, Representative images of tdTomato+ hippocampal astrocytes in home cage and fear-conditioned mice. Scale bars: top, 100 μm; bottom, 30 μm. **c**, Quantification of labelled astrocytes (n = 5 mice per group; Welch's corrected t-test, \*P = 0.023; two-tailed t-test, \*\*P = 0.0002). **d**, Schematic of the genetic system and timeline for examining Ca<sup>2+</sup> dynamics; 2P, two-photon. **e**, Representative two-photon images and GCaMP signal traces

from fear-conditioning-tagged and home-cage-tagged astrocytes. Each row in the heatmaps represents a single astrocyte. Scale bar, 10 μm. dF/F, relative fluorescence change. **f**, Quantification of Ca<sup>2+</sup> signalling parameters (n = 14 cells per group, n = 3 mice per group; two-tailed t-tests, \*\*P = 0.004 (amplitude), \*\*P = 0.002 (area under the curve (AUC)), \*\*P = 0.008 (spike width)). Data are mean ± s.e.m. except where stated otherwise. Parts **a** and **d** were created using Biorender.com.

the learning event in which they were activated. To study these ensembles, we developed a strategy that enabled genetic access to LAAs. We generated an Aldh1l1-CreER;Rosa-CAG-FSF-tdTomato reporter mouse line (FSF is Flp recognition target (FRT)-stop-FRT), which allows for astrocyte-specific and tamoxifen-inducible Cre-mediated recombination in conjunction with Flp-dependent expression of tdTomato (Fig. 2a). Next, we created a Fos-Flex-Flp AAV, which drives Flp expression in *Fos*-expressing (activated) cells and, when used with the reporter line, labels *Fos*-expressing astrocytes with tdTomato (Fig. 2a). Using this strategy, we injected the hippocampus of the reporter line with Fos-Flex-FLP AAV, treated with tamoxifen for three consecutive days, after which we subjected these mice to contextual fear conditioning or contextual exposure only, with home-cage controls (Fig. 2a). We observed a significant increase in the number of tdTomato-labelled cells that express GFAP throughout the hippocampus in all context

exposure groups relative to home-cage controls, indicating that there was successful labelling of astrocytes in an experience-dependent manner (Fig. 2b,c and Extended Data Fig. 5). We validated that all tdTomato+ cells examined expressed GFAP (Extended Data Fig. 5) and confirmed that tamoxifen administration did not affect astrocytic expression of c-Fos (Extended Data Fig. 6). It is important to note that using *Fos*, or any other single genetic entry point, may underestimate the population of astrocytes engaged by learning<sup>28</sup>. Another caveat for this labelling system is that the amount of labelling is dependent on the interval between tamoxifen injection and perfusion.

Memory consolidation involves changes to ensembles of cells associated with a memory trace<sup>1,29</sup>. Astrocytes display complex intracellular calcium signals that reflect interactions with neurons and can influence associated circuit function<sup>23,30,31</sup>. To examine whether LAAs display alterations in Ca<sup>2+</sup> activity, we co-injected

Fos–Flex–Flp and GFAP–FSF–GCaMP6 AAVs into the hippocampus of Aldh1l1-CreER mice (Fig. 2d). We injected mice with tamoxifen, after which they were either left in the home cage or fear conditioned. After allowing 3 days for sufficient expression of GCaMP6, we recorded spontaneous  $\text{Ca}^{2+}$  activity in labelled astrocytes with two-photon imaging of acute slices (Fig. 2d–f). We observed that LAAs from fear-conditioned mice displayed an overall increase in  $\text{Ca}^{2+}$  activity in the soma and main branches, including increased amplitude and duration of events.  $\text{Ca}^{2+}$  activity was also increased in microdomains of LAAs (Extended Data Fig. 5c). Notably, calcium activity in *Fos* cKO astrocytes was slightly reduced (Extended Data Fig. 4). Taken together, these findings show that elevated  $\text{Ca}^{2+}$  activity is a core feature of astrocyte ensembles activated by learning and may reflect changes in neuron–astrocyte interactions during memory consolidation.

## LAAs and engram neurons interact

We next decided to examine the interactions between learning-associated astrocytes and engram neurons associated with a single learning event. To achieve this, we developed a system that uses a tamoxifen-inducible Flp, the expression of which is driven by the *Fos* promoter (*Fos*–FlpER) (Fig. 3a and Extended Data Fig. 7). Co-injecting *Fos*–FlpER with GFAP–fDIO–tdTomato–4x6T (fDIO is FRT double-flanked inverted open reading frame) and hSyn–fDIO–EYFP enabled us to simultaneously label and map engram neurons and LAAs in wild-type mice after fear conditioning by injecting 4-hydroxytamoxifen (4-OHT) (Fig. 3b). Importantly, this tagging system labelled a proportion of astrocytes that is in line with the number that express c-Fos after fear conditioning (Extended Data Fig. 8). Moreover, astrocytes labelled during fear conditioning re-express c-Fos at rates more than 25-fold greater than for unlabelled astrocytes after a recall test, which indicates that our labelling of LAAs is highly specific to fear memory (Extended Data Fig. 8).

We used the *Fos*–FlpER system to label engram neurons and LAAs that are active during fear conditioning. We examined the proximity of engram neurons with LAAs and non-LAAs, using GFAP to estimate the territory of each astrocyte. Quantification of the volume of EYFP<sup>+</sup> processes of engram neurons in individual astrocyte territories revealed that the processes of engram neurons were preferentially localized in the domains of tdTomato<sup>+</sup> LAAs (Fig. 3c,d), with every LAA territory containing EYFP<sup>+</sup> processes. We observed no differences in the territory size between LAAs and non-LAAs. These observations indicate that there is a close association between engram neurons and the ensemble of LAAs.

Previous studies showed that fear learning increases the number of synapses between engram neurons without changing the number of synapses between non-engram neurons<sup>32</sup>. This finding indicates that engram–engram synapses are a structural substrate of memory ('synaptic engram'). To investigate whether LAAs preferentially interact with synaptic engrams, we selectively labelled engram–engram synapses using Cre-dependent enhanced GFP reconstitution across synaptic partners (eGRASP)<sup>32</sup> constructs. eGRASP uses presynaptic and postsynaptic targeted components of a split GFP to generate fluorescent puncta at synapses where both components are present. We targeted the presynaptic eGRASP component to left CA3 engram neurons by co-injection of *Fos*–CreER and Ef1 $\alpha$ –DIO–Pre–eGRASP AAVs (Fig. 3e). In the right CA1, we co-injected *Fos*–CreER and Ef1 $\alpha$ –DIO–Post–eGRASP AAVs to enable selective expression of the postsynaptic eGRASP component in CA1 engram neurons, along with *Fos*–FlpER and GFAP–fDIO–tdTomato–4x6T to label LAAs. We then fear conditioned mice and injected them with 4-OHT to label cells that were activated during learning. We examined the right CA1 in which eGRASP<sup>+</sup> puncta marking sparse engram–engram synapses were evident. We quantified the number of eGRASP puncta in the territory of individual astrocytes, as defined by GFAP, and found that tdTomato<sup>+</sup> astrocyte territories

contained significantly more eGRASP puncta, indicating that the synaptic engram is enriched in the territories of LAAs (Fig. 3f,g). These observations indicate that LAAs are well positioned to influence the activity of engram neurons. Furthermore, these findings imply that memory recall may involve coordinated interactions between unique ensembles of astrocytes and engram neurons.

## LAAs regulate neuronal engram activity

The identification of LAA ensembles that are juxtaposed with engram neurons prompted us to investigate the role of these astrocyte ensembles in circuit plasticity. Previous studies showed that activating CA1 astrocytes by the Gq pathway is sufficient to induce LTP in the CA3–CA1 circuit of the hippocampus<sup>24</sup>. To test whether activation of the relatively small ensemble of LAAs was sufficient to induce LTP, we expressed hM3D in hippocampal astrocytes tagged during fear conditioning using Aldh1l1-CreER mice injected with *Fos*–Flex–Flp and GFAP–FSF–hM3D–mCherry (Extended Data Fig. 9a,b). Using slice recordings and a subthreshold stimulus (10 stimuli at 40 Hz)<sup>33</sup>, we found that home-cage controls and LAA groups treated with saline did not induce LTP. However, when LAA groups were treated with CNO to activate hM3D, we observed a robust induction of LTP that was similar to that observed with pan-astrocyte hM3D activation (that is, CNO treated, non-fear-conditioned hM3D expressed in all astrocytes) (Extended Data Fig. 9c,d). Moreover, activating hM3D signalling in LAAs in the absence of Schaffer collateral stimulation induced a mild potentiation (Extended Data Fig. 9e). Taken together, these data indicate that the ensemble of astrocytes activated by a single learning event are capable of mediating plasticity in hippocampal circuits.

We next decided to examine whether LAA ensembles could affect the function of engram neurons. Using our activity-dependent labelling approach, we directed expression of hM3D to LAAs and EYFP to engram neurons that were active during fear conditioning (Fig. 3h). One week later, we recorded excitatory postsynaptic currents (EPSCs) from engram (EYFP<sup>+</sup>) and non-engram (EYFP<sup>-</sup>) neurons in acute slices. We obtained recordings before and after application of CNO to activate hM3D in LAAs. Activating LAAs selectively increased the frequency of EPSCs in engram neurons without affecting EPSC amplitude (Fig. 3i,j). This observation demonstrates that LAAs can regulate the synaptic activity of engram neurons.

Next, we tested whether activating LAAs increases fear engram activation at the molecular level. We expressed EYFP in engram neurons and hM3D in LAAs active during fear conditioning in a new context (context A). One week later, we injected mice with either saline or CNO (3 mg per kg, 30 min before testing) to activate hM3D-expressing astrocytes, and placed them in a different and innocuous context (context B). After 90 min, we collected brains and stained for c-Fos to determine the activation of engram neurons in context B (Fig. 3k). The CNO-injected mice had an increase in the reactivation rate of fear-tagged engram neurons (c-Fos<sup>+</sup>/EYFP<sup>+</sup>) (Fig. 3l,m and Extended Data Fig. 10a–c). Collectively, these observations indicate that LAA ensembles can regulate hippocampal circuit function by modulating the activity of engram neurons.

## LAA reactivation elicits recall

Our findings that LAA ensembles regulate hippocampal circuit plasticity and engram neuron activity raise the possibility that they may also control the recall of memories specific to the learning event in which they were activated. Therefore, we examined whether selectively reactivating LAAs tagged during fear conditioning could cause expression of adaptive behaviours (such as freezing) that mice do when experiencing fear. To achieve this, we labelled astrocyte ensembles with hM3D during fear conditioning in a new context (context A) using Aldh1l1-CreER mice injected with *Fos*–Flex–Flp and GFAP–FSF–hM3D–mCherry (Fig. 4a).

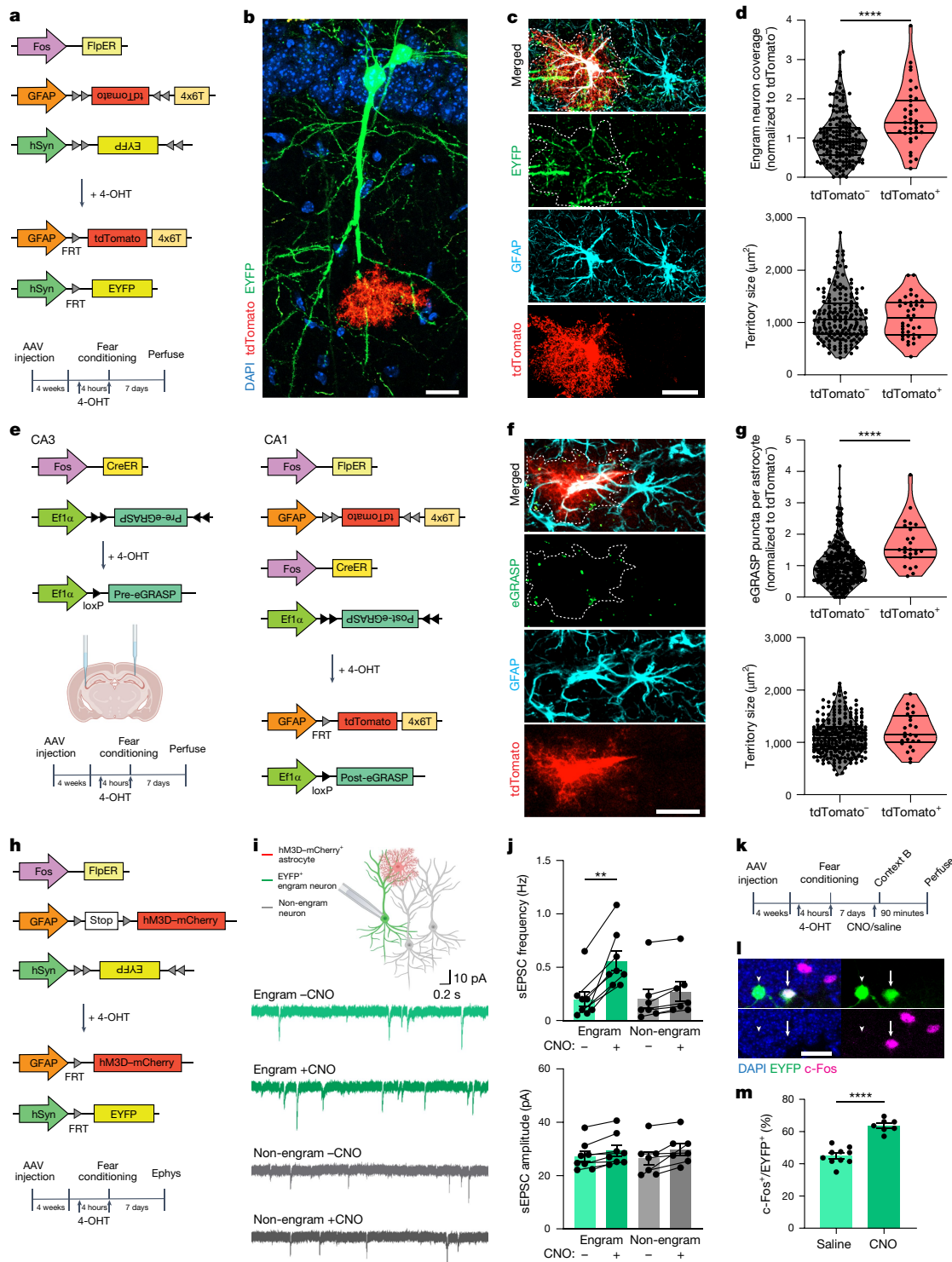


**Fig. 3 | LAAs interact with engram neurons.** **a**, Schematic for labelling LAAs and engram neurons. **b**, Image of an EYFP<sup>+</sup> engram neuron and tdTomato<sup>+</sup> LAA. Scale bar, 20 μm. **c**, Immunostaining of engram neuron processes within territories of LAA and non-LAA. Scale bar, 20 μm. **d**, Quantification of engram neuron coverage of astrocyte territories (top) and astrocyte territory size (bottom);  $n = 186$  tdTomato<sup>-</sup> astrocytes,  $n = 38$  tdTomato<sup>+</sup> astrocytes and  $n = 8$  mice; two-sided nested t-tests; top, \*\*\*\* $P < 0.0001$ ; bottom,  $P = 0.657$ ; the middle line indicates the median, and the top and bottom lines indicate quartiles. **e**, Schematic for labelling LAAs and CA3-CA1 engram-synapses. **f**, Image of eGRASP engram synapses within territories of LAA and non-LAA. Scale bar, 20 μm. **g**, Quantification of eGRASP puncta within astrocyte territories (top) and astrocyte territory size (bottom);  $n = 276$  tdTomato<sup>-</sup> astrocytes,  $n = 25$  tdTomato<sup>+</sup> astrocytes,  $n = 4$  mice; two-sided nested t-tests; top, \*\*\*\* $P < 0.0001$ ;

bottom,  $P = 0.295$ . The middle line indicates the median, and the top and bottom lines indicate quartiles. **h**, Schematic for expressing hM3D-mCherry in LAAs and EYFP in engram neurons. **i**, Diagram of recordings from engram and non-engram neurons; representative traces are shown. **j**, Quantification of EPSCs before and after CNO treatment in engram and non-engram neurons;  $n = 8$  engram neurons from 8 mice,  $n = 7$  non-engram neurons from 7 mice; top, Tukey test, \*\* $P = 0.009$ ; bottom, one-way ANOVA,  $P = 0.622$ . **k**, Timeline for examining engram neuron c-Fos expression. **l**, Immunostaining of c-Fos in EYFP<sup>+</sup> engram neurons. Arrow denotes a c-Fos<sup>+</sup>/EYFP<sup>+</sup> cell; arrowhead denotes a c-Fos<sup>+</sup>/EYFP<sup>-</sup> cell. Scale bar, 20 μm. **m**, Quantification of engram neuron activity (c-Fos<sup>+</sup>/EYFP<sup>+</sup>);  $n = 10$  saline,  $n = 7$  CNO; two-tailed t-test, \*\*\*\* $P < 0.0001$ ; data are mean  $\pm$  s.e.m. unless stated otherwise. Parts **e** and **i** were created using Biorender.com.

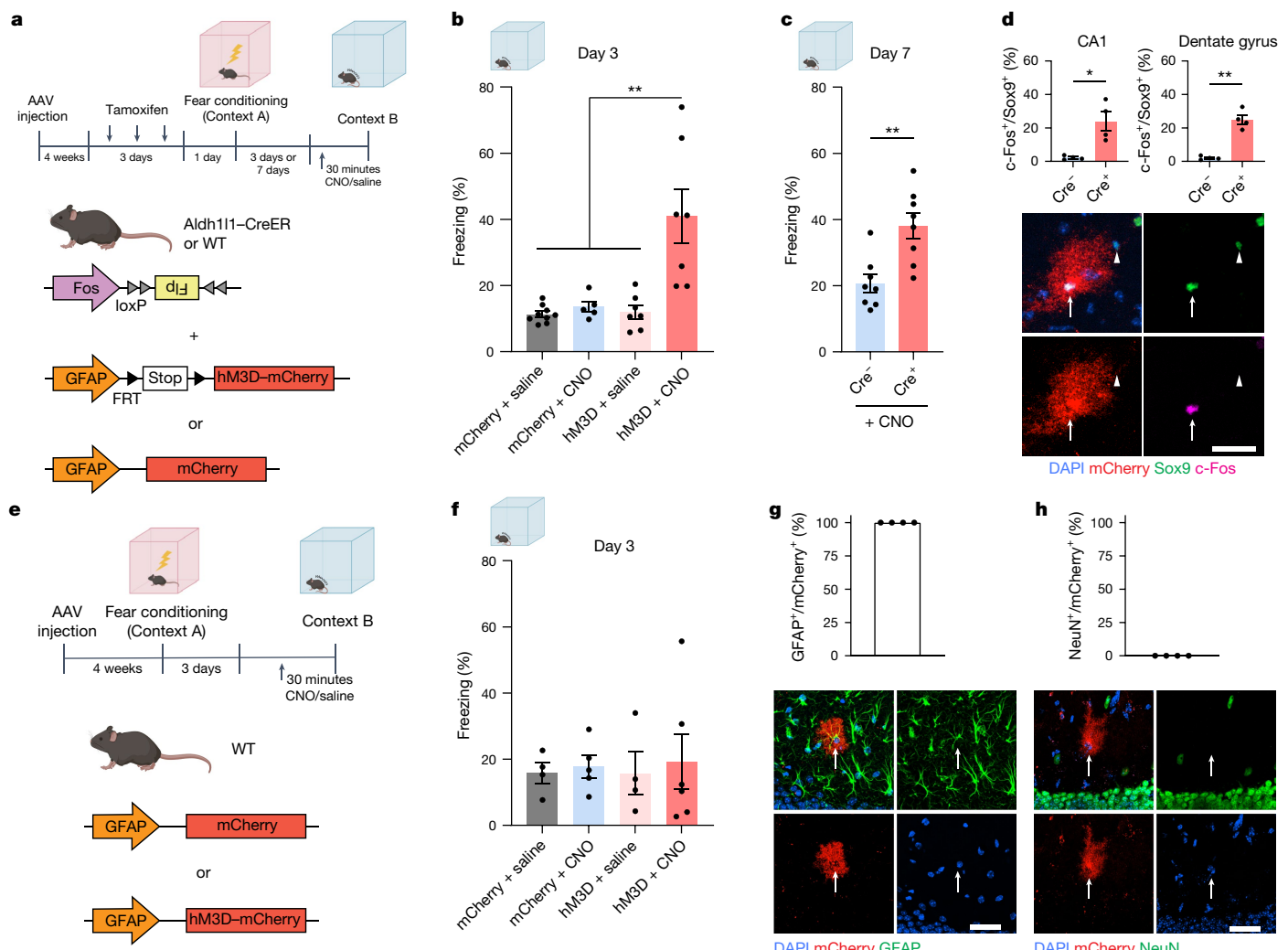


**Fig. 4 | Reactivation of LAAs elicits memory recall.** **a**, Schematic of the genetic system and timeline for tagging astrocyte ensembles active during fear learning with hM3D and subsequently reactivating them in a different context. WT, wild type. **b**, Freezing behaviour in context B after reactivation of LAAs 3 d after fear conditioning;  $n = 9$  mCherry+saline,  $n = 5$  mCherry + CNO,  $n = 7$  hM3D + saline,  $n = 7$  hM3D + CNO mice; one-way ANOVA and Dunnett's post-hoc tests, \*\* $P \leq 0.001$ . **c**, Freezing behaviour in context B after reactivation of LAAs 7 d after fear conditioning;  $n = 8$  mice injected with Fos-Flex-Flp and GFAP-FSF-hM3D-mCherry per group; two-tailed  $t$ -test, \*\* $P = 0.002$ . **d**, Quantification (top) and representative images (bottom) of c-Fos expression in Sox9<sup>+</sup> astrocytes after CNO injection in Aldh1l1-CreER<sup>+</sup> and Aldh1l1-CreER<sup>-</sup> mice;  $n = 4$  mice per

group; two-sided Welch's corrected  $t$ -tests, \* $P = 0.033$ , \*\* $P = 0.003$ . Scale bar, 20  $\mu$ m. **e**, Timeline and schematic of the genetic system for the activation of random astrocytes during recall. **f**, Freezing behaviour in context B after random astrocyte activation;  $n = 4$  mCherry + saline,  $n = 5$  mCherry + CNO,  $n = 4$  hM3D + saline,  $n = 6$  hM3D + CNO mice; one-way ANOVA,  $P = 0.974$ . **g**, Quantification (top,  $n = 4$  mice) and representative images (bottom) of hM3D-mCherry expression in GFAP<sup>+</sup> astrocytes. Scale bar, 30  $\mu$ m. **h**, Quantification (top,  $n = 4$  mice) and representative images (bottom) showing absence of hM3D-mCherry expression in neurons. Scale bar, 30  $\mu$ m. Data are mean  $\pm$  s.e.m. Parts **a–c**, **e** and **f** were created using Biorender.com.

This configuration allowed us to introduce hM3D into LAAs, enabling their subsequent reactivation. We found that reactivating LAAs by injecting CNO (3 mg per kg, 30 min before testing) either 3 d or 7 d after fear conditioning resulted in a significant increase in freezing behaviour after mice were placed in a different context (context B) (Fig. 4b–d). Furthermore, using the AAV-Fos-FlpER system, we observed a similar induction of freezing behaviour by reactivating LAAs three weeks after fear conditioning, demonstrating that the phenomenon of astrocyte ensemble-mediated memory recall is durable (Extended Data Fig. 11). We confirmed that the expression of hM3D was specific to astrocytes to exclude the possibility that increased freezing behaviour could be attributed to off-target expression of hM3D in neurons (Fig. 4g,h). Moreover, to confirm that hippocampal astrocyte activation does not non-specifically cause freezing behaviour, we bulk-labelled astrocytes with AAV-GFAP-hM3D-mCherry (or a GFAP-mCherry control; Fig. 4e). Three days after fear conditioning in context A, we placed mice

in context B after injections of saline or CNO (3 mg per kg). We found no difference in freezing across the groups (Fig. 4f), which demonstrates that stochastic astrocyte activation does not cause freezing. Taken together, these results demonstrate that selective reactivation of hippocampal astrocyte ensembles that were previously activated during fear learning is sufficient to elicit memory recall.

## LAA nuclear factor I-A is essential for recall

The observations described above indicate that LAAs exhibit distinct functional properties during experience-dependent plasticity after learning events. To examine the molecular properties of LAAs, we used the Fos-Flex-Flp AAV system and a dual reporter mouse line (Aldh1l1-CreER; Aldh1l1-GFP; Rosa-CAG-FSF-tdTomato) in which all astrocytes express GFP and Flp-expressing astrocytes also express tdTomato (Fig. 5a). With this system, we were able to label LAAs (GFP<sup>+</sup> and

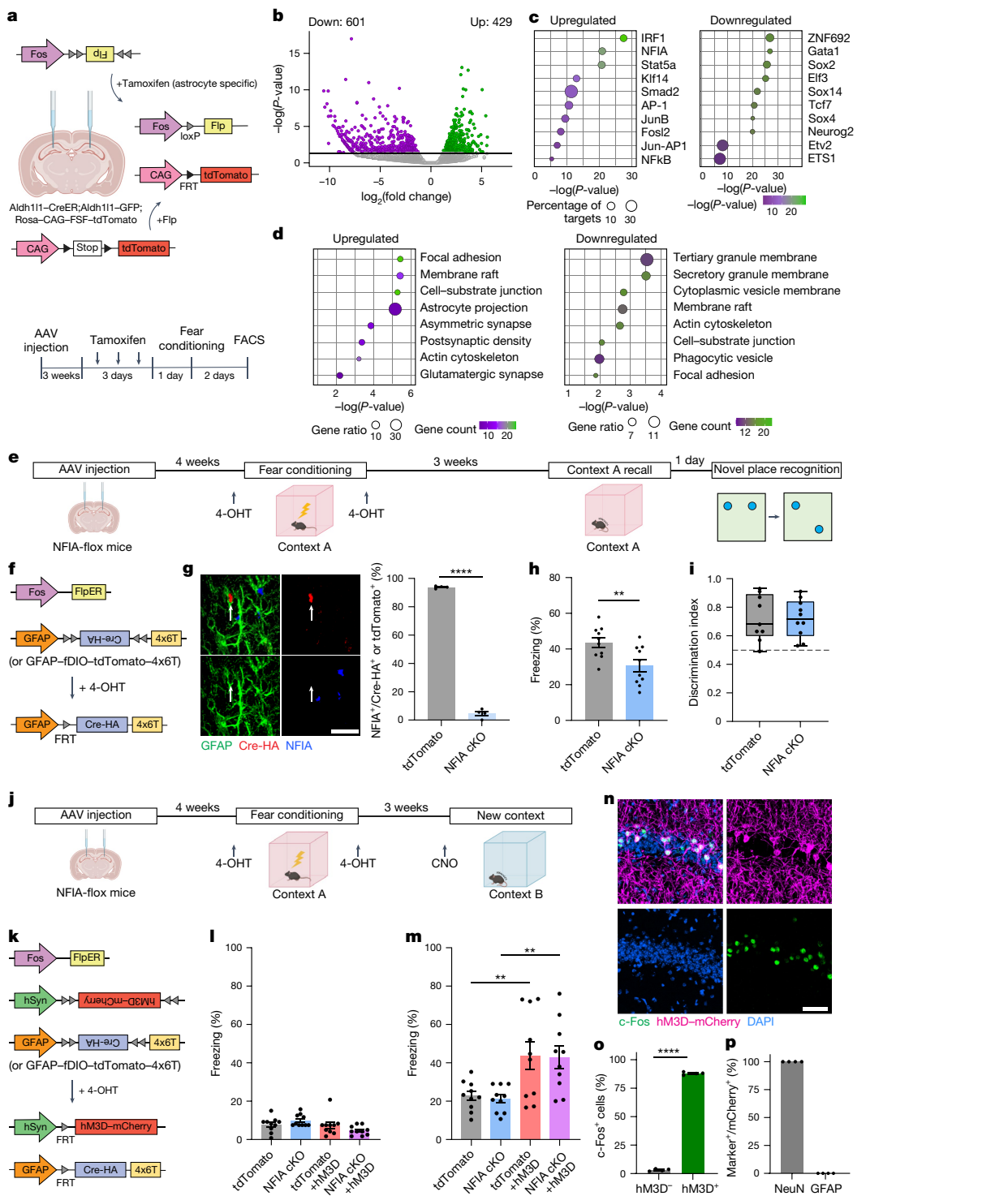


**Fig. 5 | Ensemble-specific NFIA is necessary for context-specific memory.** **a**, Schematic for labelling and sorting GFP<sup>+</sup> tdTomato<sup>+</sup> LAAs and GFP<sup>+</sup> tdTomato<sup>-</sup> non-LAAs for RNA-seq. **b**, Volcano plot depicting DEGs in LAAs and non-LAAs, showing uncorrected  $P$ -values calculated using DESeq2;  $n = 3$  biological replicates per group (hippocampus from 3 mice pooled per replicate); numbers at the top indicate number of downregulated and upregulated genes. **c**, HOMER motif analysis of transcription factor motifs enriched among upregulated (left) and downregulated (right) genes. Cumulative binomial distribution test from HOMER. **d**, Gene Ontology (GO) analysis of upregulated (left) and downregulated (right) genes.  $P$ -values were obtained using two-sided Fisher's exact test.

**e,f**, Timeline (e) and schematic (f) for knockout of NFIA in LAAs. **g**, Representative immunostaining (left) and quantification (right) of NFIA expression in tdTomato-labelled (control) and Cre-HA-labelled (NFIA cKO) astrocytes;  $n = 4$  mice per group; two-tailed  $t$ -test, \*\*\*\* $P < 0.0001$ . Scale bar, 20  $\mu$ m. **h**, Freezing during recall test in context A;  $n = 10$  mice per group; two-tailed  $t$ -test, \*\* $P = 0.009$ .

**i**, Quantification of novel place discrimination;  $n = 9$  tdTomato,  $n = 10$  NFIA cKO; two-tailed  $t$ -test,  $P = 0.960$ . **j,k**, Timeline (j) and schematic (k) for knockout of NFIA in LAAs and hM3D expression in engram neurons. **l**, Freezing before shocks in context A;  $n = 10$  mice per group; one-way ANOVA,  $P = 0.152$ . **m**, Freezing in context B 30 min after CNO injection;  $n = 10$  mice per group; one-way ANOVA,  $P = 0.002$ ; Fisher's post-hoc tests, \*\* $P \leq 0.005$ . **n**, Representative immunostaining of c-Fos expression in hM3D-mCherry<sup>+</sup> engram neurons. Scale bar, 50  $\mu$ m.

**o**, Quantification of c-Fos expression in CNO-activated hM3D-mCherry<sup>+</sup> engram neurons;  $n = 4$  mice per group; two-tailed  $t$ -test, \*\*\*\* $P < 0.0001$ . **p**, Quantification of mCherry co-labelling with NeuN or GFAP;  $n = 4$  mice. Data are mean  $\pm$  s.e.m. Parts a,e and j were created using Biorender.com.

tdTomato<sup>+</sup>) and non-LAAs (GFP<sup>+</sup> and tdTomato<sup>-</sup>). After tamoxifen treatment and fear conditioning, we used fluorescence-activated cell sorting (FACS) to purify the respective populations and performed transcriptomic RNA sequencing (RNA-seq) (Fig. 5a–d and Extended Data Fig. 12). Analysis of the differentially expressed genes (DEGs) revealed gene ontologies associated with synapse-related genes in LAAs (Fig. 5b–d and Supplementary Table 1). Subsequent HOMER transcription factor motif analysis of the DEGs showed that the nuclear factor I-A (NFIA) DNA-binding motif was enriched among genes upregulated in LAAs (Fig. 5c). We further validated that *NFIA* mRNA and protein expression were elevated in LAAs (Extended Data Fig. 13).

Previous studies have shown that astrocytic NFIA regulates hippocampal circuit function<sup>23</sup>, although it is not known whether it participates in the process of memory consolidation and recall. Moreover, whether NFIA facilitates circuit function through ensemble-specific actions is also unknown. To examine the role of NFIA in astrocyte ensembles after fear conditioning, we developed a system that enables the selective deletion of NFIA in LAAs during fear conditioning by injecting 4-OHT (Fig. 5e,f). By co-injecting AAV–Fos–FlpER with GFAP–fDIO–Cre–HA–4x6T into NFIA-flox mice, we were able to induce the deletion of NFIA in LAAs in the hippocampus after fear conditioning (Fig. 5f,g). To assess whether loss of NFIA from LAAs affected memory recall, we tested fear recall in the conditioned context (context A) and found less freezing behaviour in NFIA conditional knockout (cKO) mice compared with controls (Fig. 5h). Similarly, selectively deleting c-Fos in LAAs impaired fear recall (Extended Data Fig. 14). We next evaluated whether selective deletion of NFIA from the LAA ensemble specifically impaired fear memory, or if other hippocampus-dependent behaviours were also affected. We tested the same NFIA cKO mice on the novel place recognition task and found that they performed similarly to control mice (Fig. 5i). These findings demonstrate that memory impairment resulting from deletion of NFIA in LAAs is specific to memory recall associated with the original fear-conditioning event, whereas memory for other events remained intact. Therefore, these data indicate that a distinct ensemble of astrocytes selectively coordinates the consolidation and recall of a particular memory.

Next, we decided to determine whether fear memory recall could be rescued in NFIA cKO mice by artificially reactivating the neuronal engram. To achieve this, we co-injected AAV–Fos–FlpER and hSyn–fDIO–hM3D–mCherry with GFAP–fDIO–Cre–HA–4x6T (or GFAP–fDIO–tdTomato–4x6T) into NFIA-Flox mice (Fig. 5j,k). Four weeks after the AAV injection, mice were subjected to fear conditioning and 4-OHT treatment to label engram neurons with hM3D and delete NFIA from LAAs. We observed no differences in pre-shock freezing between groups (Fig. 5l). Three weeks later, we chemogenetically reactivated engram neurons by treating mice with CNO (3 mg per kg) 30 min before exposure to an innocuous context (context B). Importantly, hM3D-mediated reactivation of engram neurons increased freezing behaviour regardless of selective NFIA deletion in LAAs (Fig. 5m). We confirmed that CNO treatment selectively activated hM3D<sup>+</sup> engram neurons and that hM3D expression was restricted to neurons (Fig. 5n–p). These results show that activation of engram neurons can restore memory recall in mice with NFIA-deficient LAAs and indicate that recall initiated by LAA reactivation is dependent on neuronal engram function.

## Discussion

Ensembles of neurons activated by learning events control memory recall, which led us to examine whether other brain cell types also participate in memory formation, storage and recall. We found that learning events activate subsets of astrocytes in the hippocampus and that these LAA ensembles regulate memory recall, indicating that astrocytes participate in the physical manifestation and expression of memories. These findings expand on the notion that astrocytes

exhibit experience-dependent plasticity, in which astrocyte function is tuned to sensory or social experiences<sup>11,12,34</sup>, by illustrating new roles in memory consolidation and recall. Previous studies highlighted functionally diverse subpopulations of astrocytes<sup>17,19,35–37</sup>, raising the possibility that LAAs are derived from specialized subsets of astrocytes or, alternatively, represent a generalized adaptation reflecting proximity to neuronal engrams. Dissecting the ontogeny of LAAs and their interrelationships with neuronal engram ensembles will shed important light on this new mechanism underlying memory recall. In much the same way that distinct ensembles of neurons in a variety of brain regions are activated in response to a range of experiences<sup>4,38</sup>, it is likely that complementary ensembles of astrocytes are similarly activated after experience and contribute to the associated behavioural adaptations. Accordingly, the tools and methods developed in our study can be widely applied to astrocytes across a variety of experiences and brain regions.

IEGs serve as the molecular entry point for labelling the neural substrates responsible for memory recall<sup>2–5</sup>, including LAAs. Leveraging these findings, we discovered a new role for astrocytic Fos in the regulation of hippocampal circuits and learning behaviours. These observations, coupled with previous findings describing experience-dependent Sox9 transcriptional plasticity in astrocytes in the olfactory-bulb<sup>11,39</sup>, illustrate adaptive transcriptional responses in astrocytes that parallel IEG activation during neuronal plasticity<sup>40</sup>. At the molecular level, LAAs exhibit unique transcriptomes, highlighted by the upregulation of NFIA and enrichment of its prospective target genes. Astrocytic NFIA has a critical role in hippocampal circuit function<sup>23</sup> and, consistent with this, its deletion from LAAs inhibited memory recall in a context-specific manner. Astrocytes exhibit region-specific transcriptional dependencies<sup>21,36,41,42</sup>, and our observations in the hippocampus with NFIA, along with Sox9 in the olfactory system<sup>11,23,39</sup>, indicate that transcriptional plasticity in astrocytes is also mediated by these regional dependencies. Future studies will be aimed at relating these transcriptional responses to the biochemical quanta used by astrocytes as memory substrates. Collectively, our studies identify LAAs as key components of the adaptive response to learning experiences, regulating the flow of information during circuit plasticity and memory recall.

## Online content

Any methods, additional references, Nature Portfolio reporting summaries, source data, extended data, supplementary information, acknowledgements, peer review information; details of author contributions and competing interests; and statements of data and code availability are available at <https://doi.org/10.1038/s41586-024-08170-w>.

- Josselyn, S. A. & Tonegawa, S. Memory engrams: recalling the past and imagining the future. *Science* **367**, eaaw4325 (2020).
- Liu, X. et al. Optogenetic stimulation of a hippocampal engram activates fear memory recall. *Nature* **484**, 381–385 (2012).
- Ramirez, S. et al. Creating a false memory in the hippocampus. *Science* **341**, 387–391 (2013).
- Roy, D. S. et al. Brain-wide mapping reveals that engrams for a single memory are distributed across multiple brain regions. *Nat. Commun.* **13**, 1799 (2022).
- Han, J.-H. et al. Selective erasure of a fear memory. *Science* **323**, 1492–1496 (2009).
- Dallérac, G., Zapata, J. & Rouach, N. Versatile control of synaptic circuits by astrocytes: where, when and how? *Nat. Rev. Neurosci.* **19**, 729–743 (2018).
- Kofuji, P. & Araque, A. Astrocytes and behavior. *Annu. Rev. Neurosci.* **44**, 49–67 (2021).
- Allen, N. J. & Eroglu, C. Cell biology of astrocyte-synapse interactions. *Neuron* **96**, 697–708 (2017).
- Nagai, J. et al. Behaviorally consequential astrocytic regulation of neural circuits. *Neuron* **109**, 576–596 (2021).
- Soto, J. S. et al. Astrocyte-neuron subproteomes and obsessive-compulsive disorder mechanisms. *Nature* **616**, 764–773 (2023).
- Sardar, D. et al. Induction of astrocytic Slc22a3 regulates sensory processing through histone serotonylation. *Science* **380**, eade0027 (2023).
- Cheng, Y.-T. et al. Social deprivation induces astrocytic TRPA1-GABA suppression of hippocampal circuits. *Neuron* **111**, 1301–1315 (2023).
- Lawal, O., Ulloa Severino, F. P. & Eroglu, C. The role of astrocyte structural plasticity in regulating neural circuit function and behavior. *Glia* **70**, 1467–1483 (2022).

14. Fleischmann, A. et al. Impaired long-term memory and NR2A-type NMDA receptor-dependent synaptic plasticity in mice lacking c-Fos in the CNS. *J. Neurosci.* **23**, 9116–9122 (2003).
15. Katche, C. et al. Delayed wave of c-Fos expression in the dorsal hippocampus involved specifically in persistence of long-term memory storage. *Proc. Natl Acad. Sci. USA* **107**, 349–354 (2010).
16. Lacagnina, A. F. et al. Distinct hippocampal engrams control extinction and relapse of fear memory. *Nat. Neurosci.* **22**, 753–761 (2019).
17. Khakh, B. S. & Sofroniew, M. V. Diversity of astrocyte functions and phenotypes in neural circuits. *Nat. Neurosci.* **18**, 942–952 (2015).
18. Papouin, T., Dunphy, J., Tolman, M., Foley, J. C. & Haydon, P. G. Astrocytic control of synaptic function. *Philos. Trans. R. Soc. Lond. B Biol. Sci.* **372**, 20160154 (2017).
19. Endo, F. et al. Molecular basis of astrocyte diversity and morphology across the CNS in health and disease. *Science* **378**, eadc9020 (2022).
20. Kol, A. et al. Astrocytes contribute to remote memory formation by modulating hippocampal–cortical communication during learning. *Nat. Neurosci.* **23**, 1229–1239 (2020).
21. Cheng, Y.-T. et al. Inhibitory input directs astrocyte morphogenesis through glial GABA<sub>A</sub>R. *Nature* **617**, 369–376 (2023).
22. Henneberger, C., Papouin, T., Oliet, S. H. R. & Rusakov, D. A. Long-term potentiation depends on release of D-serine from astrocytes. *Nature* **463**, 232–236 (2010).
23. Huang, A. Y.-S. et al. Region-specific transcriptional control of astrocyte function oversees local circuit activities. *Neuron* **106**, 992–1008 (2020).
24. Adamsky, A. et al. Astrocytic activation generates de novo neuronal potentiation and memory enhancement. *Cell* **174**, 59–71 (2018).
25. Suthard, R. L. et al. Basolateral amygdala astrocytes are engaged by the acquisition and expression of a contextual fear memory. *J. Neurosci.* <https://doi.org/10.1523/JNEUROSCI.1775-22.2023> (2023).
26. Yap, E.-L. & Greenberg, M. E. Activity-regulated transcription: bridging the gap between neural activity and behavior. *Neuron* **100**, 330–348 (2018).
27. Gleichman, A. J., Kawaguchi, R., Sofroniew, M. V. & Carmichael, S. T. A toolbox of astrocyte-specific, serotype-independent adeno-associated viral vectors using microRNA targeting sequences. *Nat. Commun.* **14**, 7426 (2023).
28. Sun, W. et al. Spatial transcriptomics reveal neuron–astrocyte synergy in long-term memory. *Nature* <https://doi.org/10.1038/s41586-023-07011-6> (2024).
29. Chen, M. B., Jiang, X., Quake, S. R. & Südhof, T. C. Persistent transcriptional programmes are associated with remote memory. *Nature* **587**, 437–442 (2020).
30. Yu, X. et al. Reducing astrocyte calcium signaling in vivo alters striatal microcircuits and causes repetitive behavior. *Neuron* **99**, 1170–1187 (2018).
31. Ung, K., Tepe, B., Pekarek, B., Arenkiel, B. R. & Deneen, B. Parallel astrocyte calcium signaling modulates olfactory bulb responses. *J. Neurosci. Res.* **98**, 1605–1618 (2020).
32. Choi, J.-H. et al. Interregional synaptic maps among engram cells underlie memory formation. *Science* **360**, 430–435 (2018).
33. Park, H. et al. Channel-mediated astrocytic glutamate modulates hippocampal synaptic plasticity by activating postsynaptic NMDA receptors. *Mol. Brain* **8**, 7 (2015).
34. Yu, X. et al. Context-specific striatal astrocyte molecular responses are phenotypically exploitable. *Neuron* <https://doi.org/10.1016/j.neuron.2020.09.021> (2020).
35. Lin, C.-C. J. et al. Identification of diverse astrocyte populations and their malignant analogs. *Nat. Neurosci.* **20**, 396–405 (2017).
36. Morel, L. et al. Molecular and functional properties of regional astrocytes in the adult brain. *J. Neurosci.* **37**, 8706–8717 (2017).
37. de Ceglia, R. et al. Specialized astrocytes mediate glutamatergic gliotransmission in the CNS. *Nature* <https://doi.org/10.1038/s41586-023-06502-w> (2023).
38. Ghandour, K. et al. Orchestrated ensemble activities constitute a hippocampal memory engram. *Nat. Commun.* **10**, 2637 (2019).
39. Ung, K. et al. Olfactory bulb astrocytes mediate sensory circuit processing through Sox9 in the mouse brain. *Nat. Commun.* **12**, 5230 (2021).
40. Rao-Ruiz, P. et al. Engram-specific transcriptome profiling of contextual memory consolidation. *Nat. Commun.* **10**, 2232 (2019).
41. Lozzi, B., Huang, T.-W., Sardar, D., Huang, A. Y.-S. & Deneen, B. Regionally distinct astrocytes display unique transcription factor profiles in the adult brain. *Front. Neurosci.* <https://doi.org/10.3389/fnins.2020.00061> (2020).
42. Cheng, Y.-T., Woo, J. & Deneen, B. Sculpting astrocyte diversity through circuits and transcription. *Neuroscientist* <https://doi.org/10.1177/10738584221082620> (2022).

**Publisher's note** Springer Nature remains neutral with regard to jurisdictional claims in published maps and institutional affiliations.

Springer Nature or its licensor (e.g. a society or other partner) holds exclusive rights to this article under a publishing agreement with the author(s) or other rightsholder(s); author self-archiving of the accepted manuscript version of this article is solely governed by the terms of such publishing agreement and applicable law.

© The Author(s), under exclusive licence to Springer Nature Limited 2024

## Methods

### Animals

The mice were used in compliance with protocols approved by the Institutional Animal Care and Use Committee at Baylor College of Medicine. They were housed with food and water available ad libitum under a 12 h:12 h light–dark cycle in a 20–22 °C and 40–60% humidity environment. The following transgenic strains were used: Fos-flox (037115-JAX), Rosa-CAG-LSL-tdTomato (Ai14; Jackson Laboratory, 007914), Rosa-CAG-FSF-tdTomato (Ai65F; Jackson Laboratory, 032864), Aldh1l1-CreER (Jackson Laboratory, 029655), Aldh1l1-GFP (RRID:MMRRC\_011015-UCD) and NFIA-flox<sup>43</sup>. All mice were on a C57/b6 background. Transgenic strains were crossed as described in the main text. We used mice 2–6 months old of both sexes and randomly allocated littermates to groups. Experiments and analyses were done blinded to group allocation.

To induce recombination with Fos–Flex–Flp constructs, mice were injected intraperitoneally for three consecutive days with 100 mg per kg tamoxifen (Sigma, T5648) in corn oil. To induce recombination with Fos–FlpER constructs, mice were injected intraperitoneally with 50 mg per kg 4-OHT (Sigma, H6278) dissolved in 9:1 corn oil:ethanol. Two 4-OHT intraperitoneal injections were given 4 h apart, with the second dose delivered immediately after fear conditioning for mice subjected to the behavioural paradigm. For stimulation of Gq-coupled signalling by hM3D, mice were injected intraperitoneally with clozapine N-oxide (CNO; Abcam, ab141704) dissolved in saline (doses are indicated for each experiment in the text). CNO was administered 30 min before behavioural testing and 90 min before perfusion.

### Plasmid and virus production

The following plasmids were used for AAV packaging or the creation of new constructs: GFAP–Cre–4x6T (a gift from S. T. Carmichael; Addgene plasmid 196410), GFAP–hM3D–mCherry (a gift from B. Roth; Addgene plasmid 50478), hSyn–hM3D(Gq)–mCherry (a gift from B. Roth; Addgene plasmid 50474), hSyn–fDIO–EYFP (a gift from U. Gether; Addgene plasmid 154870), gfaABC1D–cyto–GCaMP6f (a gift from B. Khakh; Addgene plasmid 52925), Villinpromoter–blue–FlpOERT2 (a gift from J. Elverløv-Jakobsen; Addgene plasmid 67278), pOTTC475–pAAV–c-Fos–iRFP (a gift from B. Harvey; Addgene plasmid 47906), EF1a–fDIO–Cre–HA (a gift from E. Engel & A. Nectow; Addgene plasmid 121675), Fos–CreER (a gift from J.-H. Cho, Addgene plasmid 194643), pAAV–EWB–DIO–cyan–pre-eGRASP(p30) (a gift from B.-K. Kaang, Addgene plasmid 111583), pAAV–EWB–DIO–myriRFP670V5–P2A–post-eGRASP (a gift from B.-K. Kaang, Addgene plasmid 111585), pAAV–hSyn–Cre–P2A–tdTomato (a gift from R. Larsen, Addgene plasmid 107738), pAAV–GFAP–HA–rM3D(Gs)–IRES–mCitrine (a gift from B. Roth; Addgene plasmid 50472), Ef1a–fDIO–tdTomato (a gift from P. Jensen; Addgene plasmid 128434), pAAV–hSyn–fDIO–hM4D(Gi)–mCherry–WPRePA (a gift from U. Gether, Addgene plasmid 154867) and hSyn–fDIO–hM3D(Gq)–mCherry (a gift from U. Gether; Addgene plasmid 154868).

The following constructs were made by Gibson assembly or restriction cloning: Fos–Flex–Flp, GFAP–FSF–GCaMP6, GFAP–FSF–hM3D–mCherry, Fos–FlpER, GFAP–fDIO–tdTomato–4x6T, GFAP–fDIO–Cre–HA–4x6T, GFAP–FSF–hM4D–mCherry, GFAP–fDIO–rM3D–mCitrine and GFAP–fDIO–Cre–P2A–dTomato–4x6T.

All new constructs were verified by whole-plasmid sequencing before AAV packaging. AAVs were packaged by the Optogenetics and Viral Vectors Core at the Jan and Dan Duncan Neurological Research Institute. AAV2/9 was produced at the following titres (in genome copies per ml): GFAP–Cre–4x6T,  $7.3 \times 10^{12}$ ; GFAP–mCherry,  $3.5 \times 10^{12}$ ; GFAP–hM3D–mCherry,  $1.2 \times 10^{12}$ ; hSyn–hM3D–mCherry,  $3.5 \times 10^{12}$ ; Fos–Flex–Flp,  $9.3 \times 10^{12}$ ; GFAP–FSF–GCaMP6,  $9.3 \times 10^{11}$ ; Fos–FlpER,  $2.6 \times 10^{12}$ ; GFAP–fDIO–tdTomato–4x6T,  $2.8 \times 10^{12}$ ; hSyn–fDIO–EYFP,  $1.8 \times 10^{12}$ ; GFAP–FSF–hM3D–mCherry,  $2.3 \times 10^{12}$ ; GFAP–fDIO–Cre–HA–4x6T,

$3.7 \times 10^{12}$ ; hSyn–fDIO–hM3D–mCherry,  $2.3 \times 10^{12}$ ; CaMKIIa–hM3D–mCherry,  $3.9 \times 10^{12}$ ; Fos–CreER,  $6.7 \times 10^{12}$ ; Ef1 $\alpha$ –DIO–pre-eGRASP,  $4.0 \times 10^{12}$ ; Ef1 $\alpha$ –DIO–post-eGRASP,  $2.1 \times 10^{12}$ ; GFAP–FSF–hM4D–mCherry,  $3.9 \times 10^{12}$ ; GFAP–fDIO–rM3D–mCitrine,  $4.2 \times 10^{11}$ ; and GFAP–fDIO–Cre–P2A–dTomato–4x6T,  $4.9 \times 10^{11}$ . Retrograde AAV hSyn–hM4D mCherry (titre  $2.3 \times 10^{13}$  gene copies per ml) was purchased from Addgene (50475-AAVrg).

### AAV injection surgery

Mice were anaesthetized with isoflurane (3% induction, 2% maintenance) in oxygen and placed in a stereotaxic frame. The scalp was shaved and cleaned with alternating applications of 70% ethanol and Betadine. After a mid-line scalp incision, burr holes were drilled in the skull and 250–500  $\mu$ l AAV was injected in each target site using a pulled pipette attached to a Drummond Nanoject III. Injections were targeted bilaterally to CA1 (2.0 mm posterior, 1.4 mm lateral and 1.2 mm ventral relative to Bregma) and dentate gyrus (2.0 mm posterior, 1.4 mm lateral and 1.9 mm ventral relative to Bregma). Combinations of AAVs for each experiment are listed in the main text and figures. After injections, the scalp was sutured closed. Buprenorphine (0.6 mg per kg) was given subcutaneously 30 min before surgery and every 12 h afterwards for three days.

### Histology

Mice were perfused with phosphate buffered saline (PBS) followed by 4% paraformaldehyde in PBS. Brains were dissected and post-fixed overnight in 4% paraformaldehyde at 4 °C and then cryoprotected with 20% sucrose overnight. Brains were sectioned at 35  $\mu$ m with a cryostat.

For immunostaining, sections were washed three times in PBS and then incubated for 1 h in PBS with 0.25% Triton and 10% donkey serum (blocking buffer), then incubated overnight at room temperature with primary antibodies. The following primary antibodies were used: rat anti-c-Fos (1:5,000; Synaptic Systems, 226 017), guinea-pig anti-Cre (1:500; Synaptic Systems, 257 004), chicken anti-GFAP (1:1,000; abcam, ab4674), rabbit anti-GFAP (1:1,000; DAKO, Z0334), rabbit anti-HA (1:500; Roche, 11867423001), rabbit anti-NeuN (1:2,000; Millipore, MABN140), rabbit anti-NFIA (1:500; Sigma, HPA006111), rabbit anti-RFP (1:500; Rockland, 600-401-379) and rabbit anti-Sox9 (1:500; Millipore, AB5535). Sections were then washed three times in PBS followed by incubation with secondary antibodies (1:500) in blocking buffer for 1 h. The following secondary antibodies were used: Alexa Fluor 488-conjugated donkey anti-chicken (Jackson ImmunoResearch, 703-545-155), Alexa Fluor 647-conjugated donkey anti-chicken (Jackson ImmunoResearch, 703-605-155), Alexa Fluor 594-conjugated donkey anti-guinea-pig (Jackson ImmunoResearch, 706-585-148), Alexa Fluor 488-conjugated donkey anti-rabbit (Jackson ImmunoResearch, 711-545-152), Alexa Fluor 594-conjugated donkey anti-rabbit (Jackson ImmunoResearch, 711-585-152), Alexa Fluor 647-conjugated donkey anti-rabbit (Jackson ImmunoResearch, 711-605-152), Alexa Fluor 488-conjugated donkey anti-rat (Jackson ImmunoResearch, 712-545-153), Alexa Fluor 594-conjugated donkey anti-rat (Jackson ImmunoResearch, 712-585-153) and Alexa Fluor 647-conjugated donkey anti-rat (Jackson ImmunoResearch, 712-605-153). Sections were washed three more times in PBS before mounting and cover-slipping.

### Confocal imaging and analysis

Confocal images were acquired with a Zeiss LSM 880 laser scanning confocal microscope with  $\times 20$  air,  $\times 40$  oil or  $\times 63$  oil objective lens. Images were taken with steps of 1–2  $\mu$ m in the z plane and a pixel resolution of  $1,024 \times 1,024$  or  $2,048 \times 2,048$ . Images were quantified using ImageJ/Fiji (v.1.54 f) by experimenters blind to group identity. Cell numbers were quantified manually using the multi-point selection tool. For examination of c-Fos expression in astrocytes, we excluded analysis of the subgranular zone owing to expression of the astrocyte marker Sox9 in neural stem cells in this region. For quantification of

# Article

EYFP<sup>+</sup> neuron coverage of GFAP<sup>+</sup> astrocyte territories, maximum intensity z projections were created encompassing the territory of a given astrocyte. The polygon selection tool was used to trace the territory of each astrocyte based on the GFAP channel. Each region-of-interest selection was applied to the corresponding region in the thresholded EYFP channel, and the area fraction of EYFP<sup>+</sup> structures was computed. To account for regional differences in neuronal labelling density and differences in the laser power needed to image different neurons, the area fraction from each astrocyte was normalized to the mean of non-LAs (tdTomato<sup>-</sup>) for each image. The area measurement output was used to measure territory size. The eGRASP puncta were counted in the 3D territory of each astrocyte based on the GFAP channel. We used 2D projections to measure astrocyte territory based on the GFAP channel. Data were taken as the number of puncta (in 3D space) per astrocyte 2D territory. To account for regional variation in the number and proximity of labelled neurons, and differences in the fluorescence intensity, the number of puncta was normalized to the mean of non-LAs (tdTomato<sup>-</sup>) for each image. A caveat of this analysis is that an astrocyte may not functionally interact with every eGRASP<sup>+</sup> synapse in its territory. For fluorescence quantification, the integrated density was measured from manually drawn regions of interest.

## Contextual fear conditioning

The fear-conditioning chamber (context A) was a 25 cm × 35 cm arena with a metal grid floor. The alternative context (context B) was a 25 cm × 45 cm arena with a plastic floor. The arenas had different patterns on some walls as visual cues. Context A was cleaned with 35% isopropyl alcohol and context B was cleaned with 70% ethanol to give the contexts different scents. A fan provided approximately 65 dB of ambient noise for both chambers. Mice were recorded from above during all behavioural sessions.

For fear conditioning, mice were placed into context A for 5 min. Mice were allowed to explore the chamber for the first 120 s. Then, 1.5 mA foot shocks lasting 2 s were delivered at 120 s, 180 s and 240 s after mice were initially placed in the chamber. Mice were removed from the chamber 60 s after the final foot shock and returned to their home cage. For subsequent tests, mice were placed into context A or context B for 5 min. Videos were manually scored for freezing behaviour by a blinded investigator. Freezing was defined as the absence of movement, with the exception of breathing-related movement, lasting more than 1 s.

## Novel place recognition

Mice were placed in a square arena (40 cm × 40 cm) with two identical objects (cylinders 12 cm tall) in adjacent quadrants. Mice were trained on three consecutive days for 10 min each day to learn the position of the objects. The arena had distinct shapes on certain walls as orientation cues. On the testing day, the location of one object was moved to a different quadrant. Mice were placed in the arena for 5 min and recorded from above. The discrimination index, which is a measure of spatial memory performance, was calculated as: (time spent investigating an object in a new place – time spent investigating an object in its original place) / total time exploring either object.

## Acute slice preparation

Mice were anaesthetized deeply using isoflurane and decapitated. The brain was dissected and placed in ice-cold oxygenated (95% O<sub>2</sub>, 5% CO<sub>2</sub>) cutting solution that contained 130 mM NaCl, 24 mM NaHCO<sub>3</sub>, 1.25 mM NaH<sub>2</sub>PO<sub>4</sub>, 3.5 mM KCl, 1.5 mM CaCl<sub>2</sub>, 1.5 mM MgCl<sub>2</sub> and 10 mM D(+)-glucose, pH 7.4. A vibratome was used to take 300-μm hippocampal sections, which were transferred to oxygenated artificial cerebrospinal fluid solution (ACSF; 125 mM NaCl, 25 mM glucose, 25 mM NaHCO<sub>3</sub>, 2.5 mM KCl, 2 mM CaCl<sub>2</sub>, 1.25 mM NaH<sub>2</sub>PO<sub>4</sub> and 1 mM MgCl<sub>2</sub>, pH 7.3, 310–320 mOsm). Slices were then recovered in oxygenated ACSF for at least 1 h before recording or imaging.

## Slice electrophysiology

Hippocampal slices were prepared as above and then acclimated at room temperature for at least 1 h with continuous perfusion of oxygenated ACSF. LTP was induced by theta burst stimulation (TBS; 10 trains of 4 half-maximal stimuli at 100 Hz with a 200 ms interval) onto the Shaffer collateral pathway. Subthreshold stimulation was 10 pulses at 40 Hz (ref. 33). We measured fEPSPs in the CA1 stratum radiatum. The recording pipette was filled with 1 M NaCl solution. The fEPSPs were calculated as the slope of the response (mV/ms) and normalized to the average of the baseline. The final potentiation was calculated by averaging the last 5 min of responses. Whole-cell recording was done with pCLAMP10 and a Multi-Clamp 700B amplifier (Axon Instruments, Molecular Devices) from hippocampal CA1 neurons. The holding potential was -60 mV. The pipette resistance was typically 5–8 MΩ. The pipette was filled with an internal solution: 135 mM CsMeSO<sub>4</sub>, 8 mM NaCl, 10 mM HEPES, 0.25 mM EGTA, 1 mM Mg-ATP, 0.25 mM Na<sub>2</sub>-GTP, 30 mM QX-314, pH adjusted to 7.2 with CsOH (278–285 mosM) for EPSC measurement; or 135 mM CsCl, 4 mM NaCl, 0.5 mM CaCl<sub>2</sub>, 10 mM HEPES, 5 mM EGTA, 2 mM Mg-ATP, 0.5 mM Na<sub>2</sub>-GTP, 30 mM QX-314, pH adjusted to 7.2 with CsOH (278–285 mosM) for IPSC measurement. Spontaneous EPSCs were measured in the presence of a GABAAR antagonist, bicuculline (20 μM, Tocris). The IPSCs were measured in the presence of ionotropic glutamate-receptor antagonists, APV (50 μM, Tocris) and CNQX (20 μM, Tocris). Electrical signals were digitized and sampled at intervals of 50 ms with Digidata 1550B and Multiclick 700B amplifier (Molecular Devices) using pCLAMP (v.10.7) software. Data were filtered at 2 kHz. The recorded current was analysed using ClampFit (v.10.7) software.

## Calcium imaging and analysis

Acute slices were prepared as described above. Slices were maintained in oxygenated ACSF with a perfusion system. Calcium traces were recorded using a two-photon microscope (LSM 7MP, Zeiss) equipped with a Coherent Chameleon Ultra (II) Ti-sapphire laser tuned to 900 nm and a ×20, 1.0 NA water-immersion Zeiss objective lens. GCaMP signals were recorded for 3–5 min per trial at 1,024 × 1,024 pixel resolution and 1 Hz temporal resolution from astrocytes at depths of approximately 30 μm below the surface. All multiphoton imaging experiments were done within 4 h of slicing. Images were quantified using GEIQuant<sup>44</sup>, ImageJ (v.54 f) and Clampfit (v.10.7) software. The region-of-interest detection for soma and main processes or micro-domains was done in a semi-automated manner using the GEIQuant algorithm as previously described<sup>44</sup>. The amplitude, area under the curve and frequency values of GCaMP signals were computed using Clampfit. Spike width was calculated as the full width at half-maximum for each spike.

## Tissue dissociation and FACS

Mice were perfused with cold saline and hippocampi were dissected on ice. Hippocampi from three mice were pooled per replicate and dissociated as previously described<sup>35</sup>. Dissociated GFP<sup>+</sup> tdTomato<sup>-</sup> and GFP<sup>+</sup> tdTomato<sup>+</sup> astrocytes, and GFP<sup>-</sup> tdTomato<sup>-</sup> cells, were sorted using a Becton Dickinson FACSAria II with BD FACSDiva software. Samples were sorted using a 70 μm nozzle at a pressure of 70 p.s.i. After singlet gating with forward and side scatter, singlet events were assessed for GFP and tdTomato fluorescence. Non-fluorescent brain tissue was used as a negative control to set the double-negative population gate. We also performed single-colour controls to establish the ideal voltage, potential compensation and gating. The GFP signal was detected with a 488 nm laser, through a 505-nm long-pass filter and a 530/30 detector. The tdTomato signal was detected with a 561 nm laser, through a 570-nm long-pass filter and a 585/51 detector. We collected 100,000 events of each type into 1.5 ml tubes containing Qiagen lysis buffer. Samples were then frozen at -80 °C until RNA extraction.

## RNA extraction, library preparation and sequencing

RNA was extracted from sorted cells using an RNeasyMicro kit (4004, QIAGEN). RNA integrity (RINR8.0) was assessed using a high-sensitivity RNA analysis kit (DNF-472-0500, Agilent) on a 12-capillary fragment analyser. cDNA synthesis and Illumina sequencing libraries with 8-base-pair single indices were constructed from 10 ng total RNA using a Revelo RNA-seq high-sensitivity kit (30184149, Tecan). The resulting libraries were validated using a standard-sensitivity NGS fragment analysis kit (DNF-473-0500) on a 12-capillary fragment analyser and quantified using a Quant-it double-stranded DNA assay kit (Q33120). Equal concentrations (2 nM) of libraries were pooled and processed for paired-end (R1, 75; R2, 75) sequencing of approximately 40 million reads per sample using a High Output v.2 kit (FC-404-2002, Illumina) on an Illumina NextSeq 550 following the manufacturer's instructions.

## RNA-seq analysis

Sequencing files from each flow-cell lane were downloaded and the resulting fastq files were merged. Quality control was done using fastQC (v.0.10.1) and MultiQC (v.0.9)<sup>45</sup>. Reads were mapped to the mouse genome mm10 assembly using STAR (v.2.5.0a)<sup>46</sup>. RNA-seq data were analysed and plotted as previously described<sup>23</sup>. DESeq2 (v.1.20.0) was used for both differential gene-expression analysis (Wald test) and read-count normalization. We defined DEGs as those with normalized reads per million greater than five in at least two of the replicates and expression fold-change more than 1.5 at  $P < 0.01$ . Gene ontologies associated with DEGs were determined using Enrichr. Motif analysis was done using hypergeometric optimization of motif enrichment (HOMER v.4.10) to identify transcription-factor motifs that were enriched near the transcription start site of differentially expressed genes.

## Quantitative PCR with reverse transcription

This was done on cDNA libraries using Quantabio Perfecta SYBR Green Fast Mix (95072-012) on a Roche Light Cycler 480 instrument. Reactions were set up using 2 ng cDNA, 250 nM primers and 1× SYBR mix. Quantitative PCR was done for 30 s at 95 °C, 40 cycles at 95 °C for 5 s and 60 °C for 30 s, with subsequent melting-curve analysis. Expression of transcripts of target genes was normalized to GAPDH. The primers used for quantitative PCR with reverse transcription are as follows: GAPDH (forward 5'-TGGCCTTCCGTGTTCTAC-3', reverse 5'-GAGTTGCTGTTGAAGTCGCA-3'), Tuj1 (forward 5'-TAGACCCCAGC GGCAACTAT-3', reverse 5'-GTTCCAGGTTCCAAGTCCACC-3'), NFIA (forward 5'-GAAGCGCATGTCGAAAGAAGA-3', reverse 5'-GGCGGAGG CAGTCAATTCTC-3') and Sox9 (forward 5'-AGTACCCGCATCTGC ACAAC-3', reverse 5'-ACGAAGGGTCTCTCTCGCT-3').

## Statistical analysis

All sample sizes and statistical tests are mentioned in the figure legends, with  $\alpha$  set at  $P < 0.05$ . Graphpad Prism (v.10) was used for all statistical

analyses. Independent samples were compared with two-tailed  $t$ -tests. Variance was assessed with  $F$ -tests, and Welch's corrected  $t$ -tests were used when variance was significantly different. One-way ANOVA and nested  $t$ -tests were used as described for each figure. Post-hoc tests were used after significant ANOVA, as described for the figures.

## Reporting summary

Further information on research design is available in the Nature Portfolio Reporting Summary linked to this article.

## Data availability

RNA-sequencing data have been deposited at the NCBI GEO under accession number GSE254016. All other data are available from the corresponding author on reasonable request. Source data are provided with this paper.

43. Scavuzzo, M. A. et al. Pancreatic cell fate determination relies on Notch ligand trafficking by NFIA. *Cell Rep.* **25**, 3811–3827 (2018).
44. Srinivasan, R. et al. Ca<sup>2+</sup> signaling in astrocytes from *Ip3r2*<sup>-/-</sup> mice in brain slices and during startle responses *in vivo*. *Nat. Neurosci.* **18**, 708–717 (2015).
45. Ewels, P., Magnusson, M., Lundin, S. & Käller, M. MultiQC: summarize analysis results for multiple tools and samples in a single report. *Bioinformatics* **32**, 3047–3048 (2016).
46. Dobin, A. et al. STAR: ultrafast universal RNA-seq aligner. *Bioinformatics* **29**, 15–21 (2013).

**Acknowledgements** This work was supported by US National Institutes of Health grants R35-NS132230, R21-MH134002 and R01-AG071687 to B.D. M.R.W. is supported by American Heart Association grant AHA-23POST1019413. W.K. is supported by the National Research Foundation of Korea (RS-2024-00405396). We thank the David and Eula Wintermann Foundation for support. We thank the Optogenetics and Viral Vectors/Neuroconnectivity Core (supported by US National Institutes of Health grant U54-HD08309) at the Jan and Dan Duncan Neurological Research Institute for virus production. This research was supported by the Eunice Kennedy Shriver National Institute of Child Health & Human Development of the National Institutes of Health under award P50HD103555 for use of the Microscopy Core facilities and the Animal Phenotyping & Preclinical Endpoints Core facilities. The schematics in the figures were created using Biorender.com.

**Author contributions** W.K., M.R.W. and B.D. conceived the project and designed the experiments. W.K. and M.R.W. generated the AAV viral constructs and performed the brain injections, behavioural studies, analysis of brain tissue and RNA-seq. J.W. did the electrophysiological recordings. Y.K., K.Y., S.M. and D.S. assisted with the RNA-seq studies and bioinformatics analysis. K.Y., E.M. and Y.K. assisted with analysis and imaging of brain tissue. M.R.W., W.K. and B.D. wrote the manuscript. For CV purposes, M.R.W. and W.K. can be interchanged in the author list because they contributed equally, with the order decided by tossing a coin.

**Competing interests** The authors declare no competing interests.

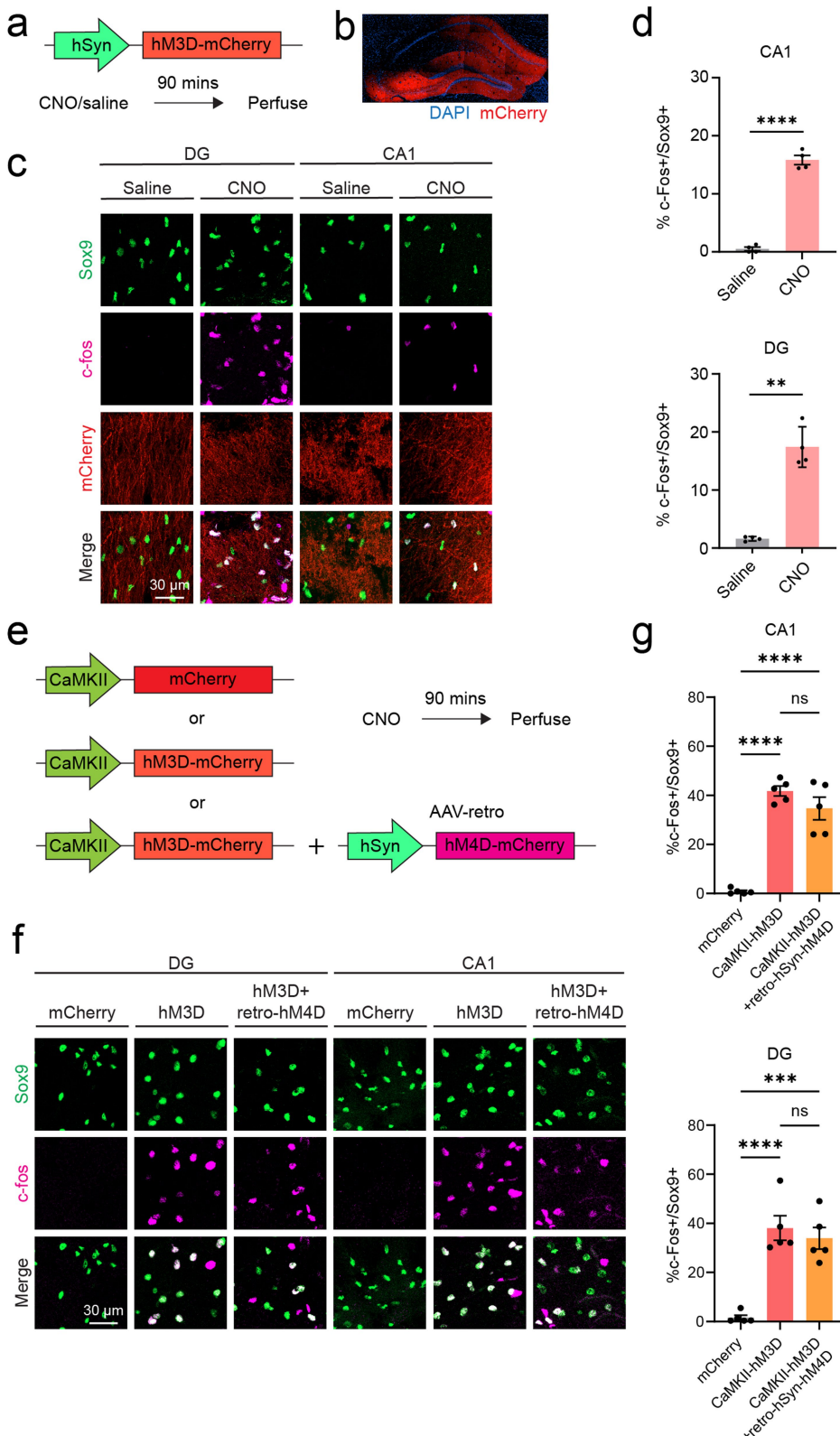
## Additional information

**Supplementary information** The online version contains supplementary material available at <https://doi.org/10.1038/s41586-024-08170-w>.

**Correspondence and requests for materials** should be addressed to Benjamin Deneen.

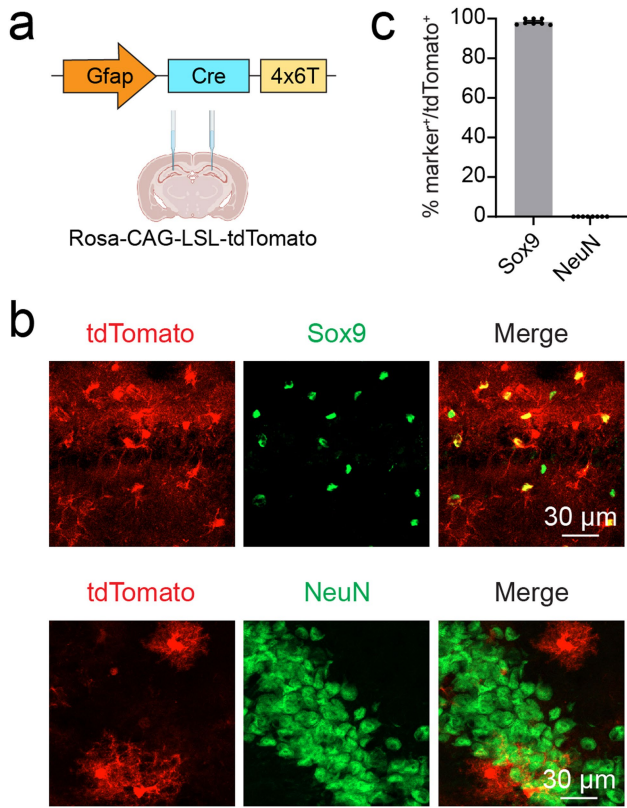
**Peer review information** *Nature* thanks C. Justin Lee, Gertrudis Perea and the other, anonymous, reviewer(s) for their contribution to the peer review of this work. Peer review reports are available.

**Reprints and permissions information** is available at <http://www.nature.com/reprints>.



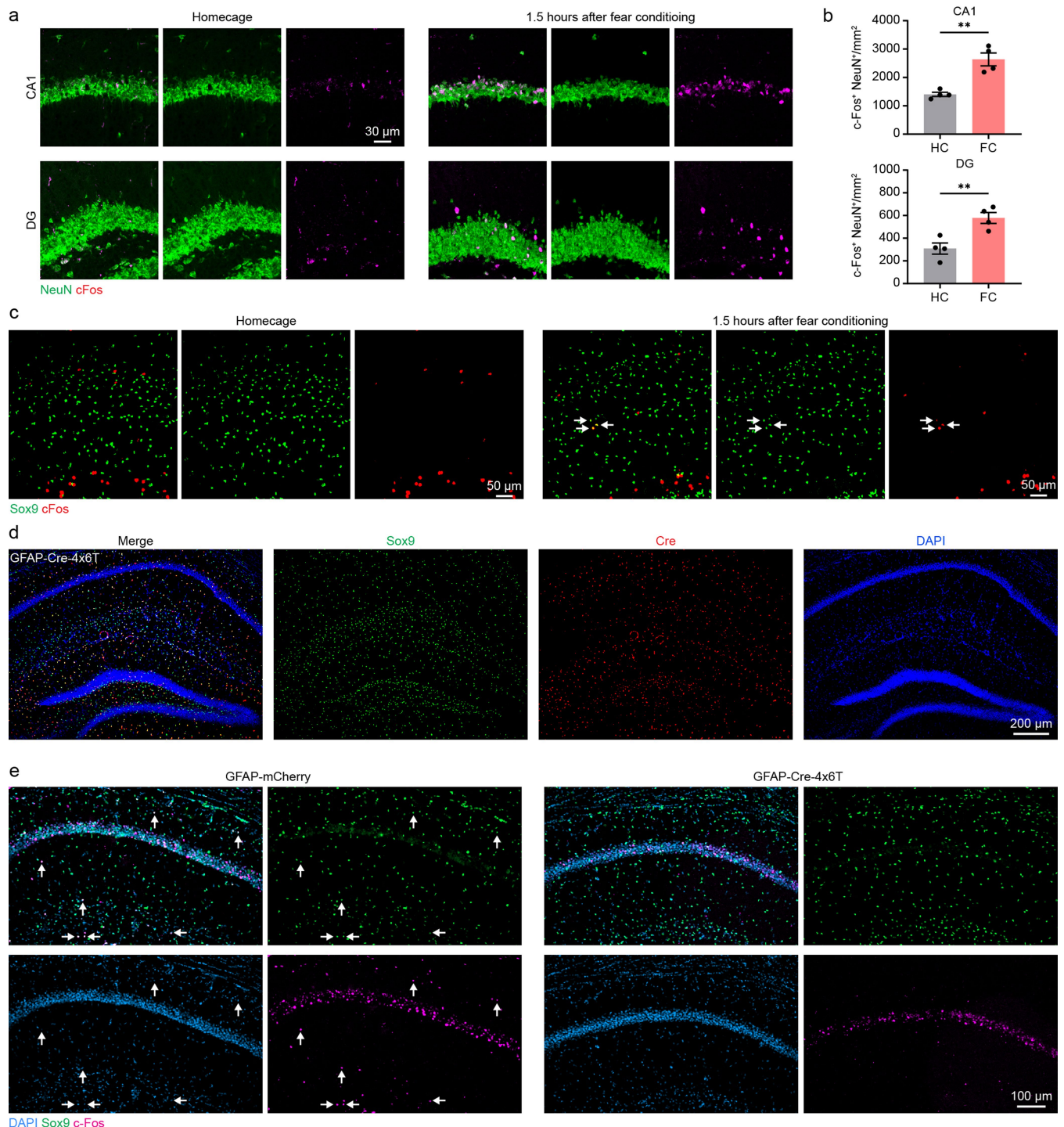
**Extended Data Fig. 1 | Chemogenetic activation of hippocampal neurons induces c-Fos expression in a subset of astrocytes.** **a.** Genetic system and timeline for chemogenetic activation of dentate gyrus neurons. Retrograde AAV-hSyn-hM4D-mCherry was used to inhibit inputs. **b.** Representative image of hM3D-mCherry labeling in the hippocampus (representative of 3 mice). **c.** Representative immunostaining of c-Fos expression in hippocampal astrocytes. **d.** Quantification of c-Fos+ Sox9+ astrocytes following saline or CNO injection ( $n = 4$  mice per group, upper panel: two-tailed t test, \*\*\*\* $P < 0.0001$ , lower panel: two-sided Welch's corrected t test, \*\* $P = 0.003$ ).

**e.** Genetic system and timeline for chemogenetic activation of excitatory dentate gyrus neurons. Retrograde AAV-hSyn-hM4D-mCherry was used to inhibit inputs. **f.** Representative immunostaining of c-Fos expression in hippocampal astrocytes. **g.** Quantification of c-Fos+ Sox9+ astrocytes following CNO injection ( $n = 5$  mice per group, upper panel: one-way ANOVA ( $P < 0.0001$ ) and Tukey tests, \*\*\*\* $P < 0.0001$ , lower panel: one-way ANOVA ( $P < 0.0001$ ) and Tukey tests, \*\*\* $P = 0.0002$ , \*\*\*\* $P < 0.0001$ ). Data are mean  $\pm$  SEM.



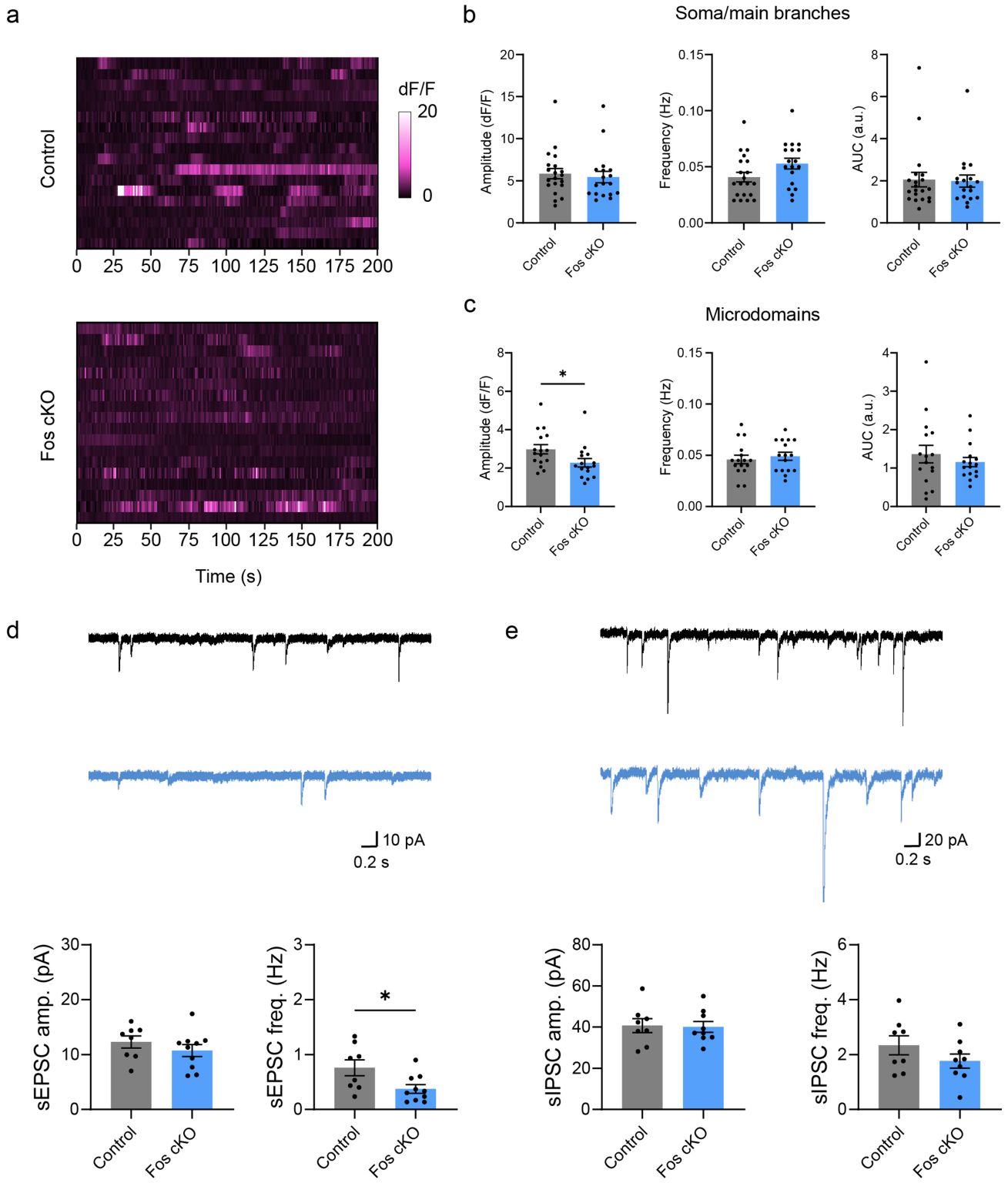
**Extended Data Fig. 2 | Specific targeting of astrocytes with AAV-GFAP-Cre-4x6T.** **a.** Schematic of genetic system for testing specificity of AAV-GFAP-Cre-4x6T in tdTomato Cre reporter mice. **b.** Representative immunostaining for Sox9+ astrocytes and NeuN+ neurons. **c.** Quantification of overlap between tdTomato and Sox9 or NeuN ( $n = 8$  mice). Data are mean  $\pm$  SEM. Panel a was created using Biorender.com.

# Article



**Extended Data Fig. 3 | Additional characterization of c-Fos expression and Fos cKO.** **a.** Representative images of c-Fos expression in hippocampal neurons from mice left in homecage or 90 min after fear conditioning. **b.** Quantification of neuronal c-Fos expression ( $n = 4$  mice per group (HC = homecage, FC = fear conditioning), two-tailed t tests,  $^{**}P = 0.002$  (upper), 0.008 (lower)). **c.** Representative images encompassing portions of stratum radiatum, stratum lacunosum, and stratum moleculare of Sox9 and c-Fos. Arrows indicate c-Fos+

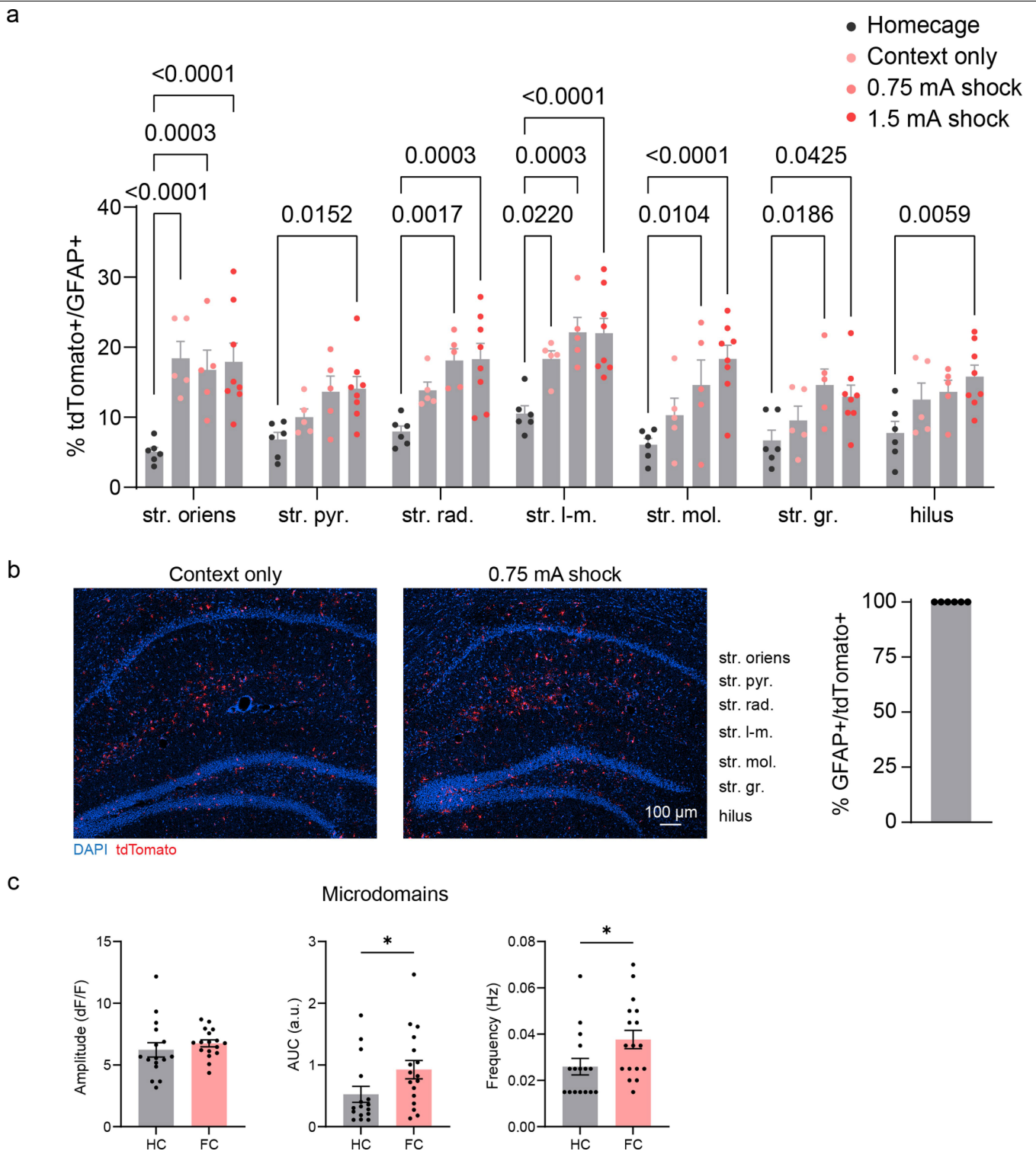
Sox9+ cells. Representative of 4 mice/group. **d.** Representative images showing astrocytic expression of Cre following injection of AAV-GFAP-Cre-4x6T. Images were processed with a dehaze filter. Representative of 4 mice. **e.** Representative images of astrocytic c-Fos expression from GFAP-mCherry and GFAP-Cre-4x6T injected mice. Arrows indicate c-Fos+ Sox9+ cells. Representative of 8 mice/group. Data are mean  $\pm$  SEM.



**Extended Data Fig. 4 | Calcium imaging and electrophysiology in Fos cKO mice.** **a.** Calcium signal traces from control and Fos cKO astrocytes. Each row in the heatmaps represents a single astrocyte ( $n = 20$  control, 18 Fos cKO astrocytes,  $n = 3$  mice per group). **b-c.** Quantification of calcium signaling parameters in soma/major branches (**b**) and microdomains (**c**) ( $n = 20$  control, 18 Fos cKO astrocytes,  $n = 3$  mice per group for some/main branches;  $n = 16$

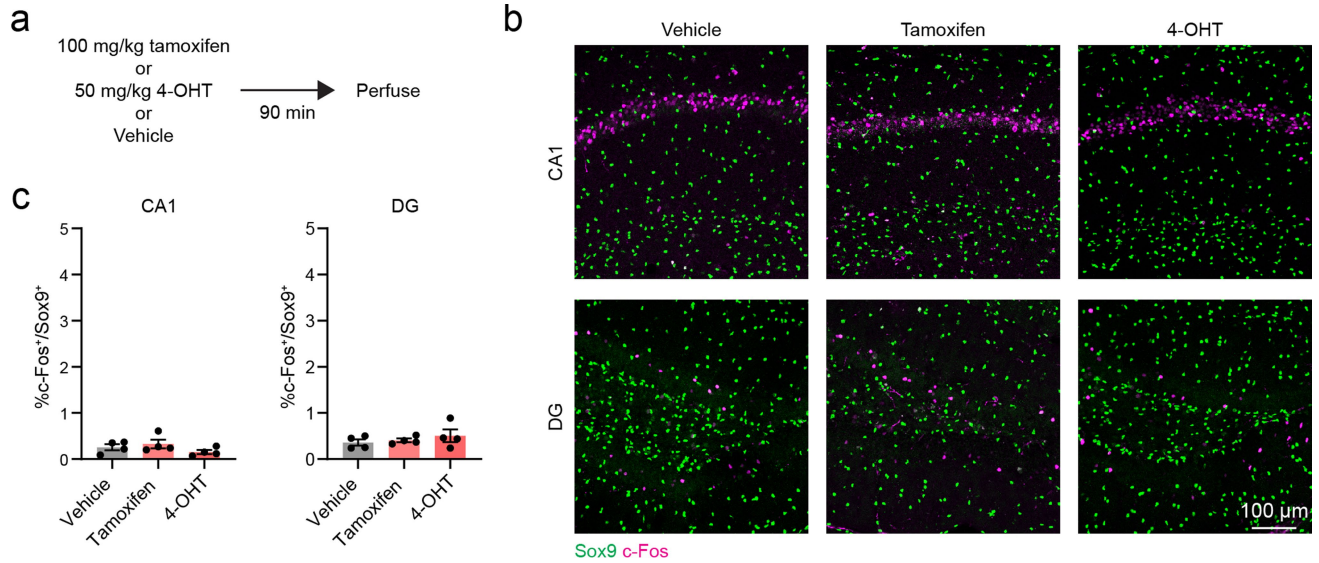
astrocytes,  $n = 3$  mice per group for microdomains). Two-tailed t test, \* $P = 0.038$ . **d.** Representative traces and quantification of sEPSCs in control ( $n = 8$ ) and Fos cKO ( $n = 10$ ) mice. Two-tailed t test, \* $P = 0.026$ . **e.** Representative traces and quantification of sIPSCs in control ( $n = 8$ ) and Fos cKO ( $n = 9$ ) mice. Data are mean  $\pm$  SEM.

# Article



**Extended Data Fig. 5 | Additional characterization of learning-associated astrocyte distribution and microdomain calcium activity.** **a.** Quantification of learning-associated astrocytes across hippocampal layers (see Fig. 2). Comparisons on graph are P values from Dunnett's tests. N = 6 homecage, N = 5 context only, N = 5 0.75 mA shock, N = 8 1.5 mA shock mice. **b.** Representative images of tdTomato+ learning-associated astrocytes in the hippocampus and quantification of co-labeling with GFAP. Str. oriens = stratum oriens,

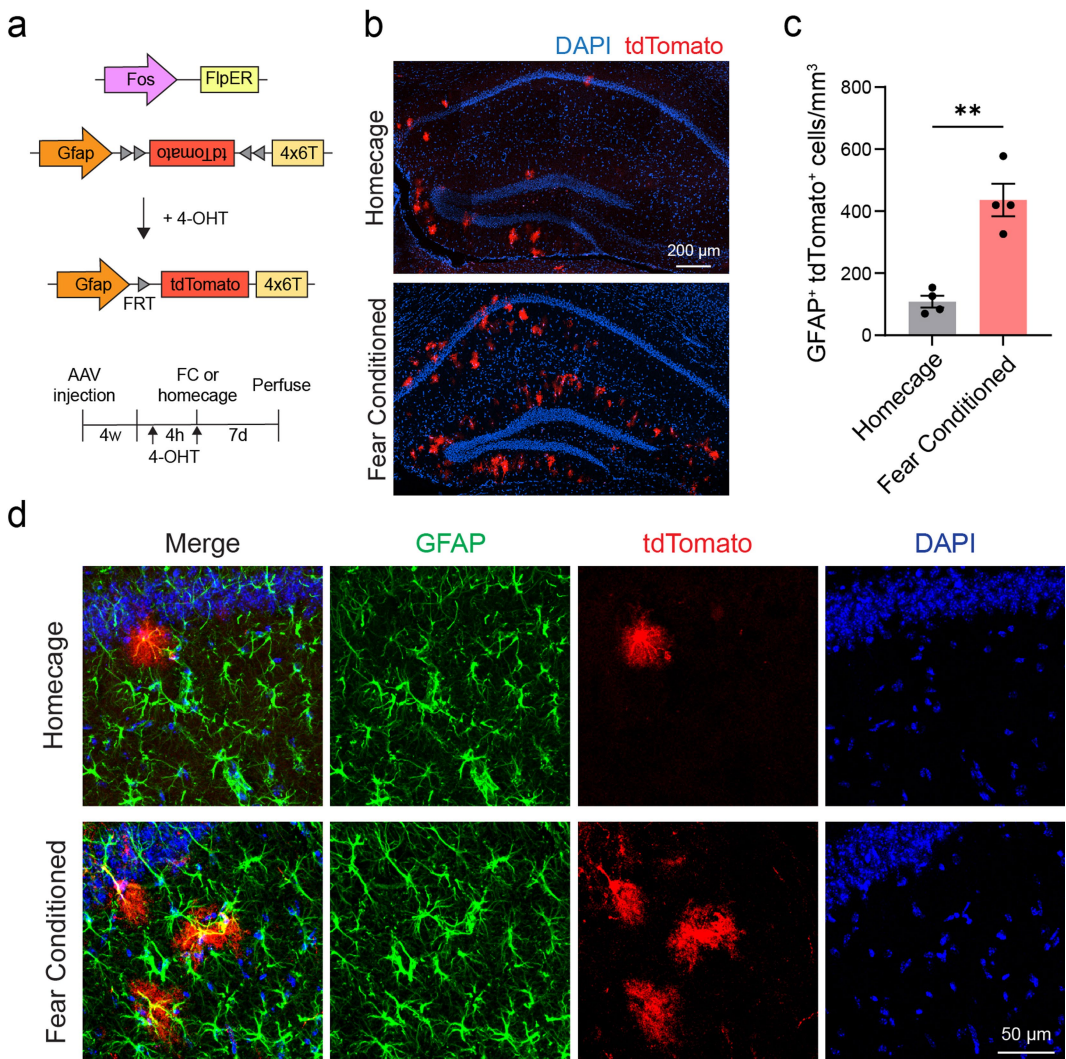
str. pyr. = stratum pyramidale, str. rad. = stratum radiatum, str. l-m. = stratum lacunosum-moleculare, str. mol. = stratum moleculare of the dentate gyrus, str. gr. = stratum granulosum. Representative of 5 mice each. **c.** Quantification of microdomain calcium activity parameters related to Fig. 2d,e. Middle panel: two-tailed Mann Whitney test, \*P = 0.030. Right panel: two-tailed t test, \*P = 0.036. n = 16 homecage and 17 fear conditioning cells from 3 mice per group. Data are mean  $\pm$  SEM.



**Extended Data Fig. 6 | Tamoxifen does not affect astrocytic c-Fos expression.**

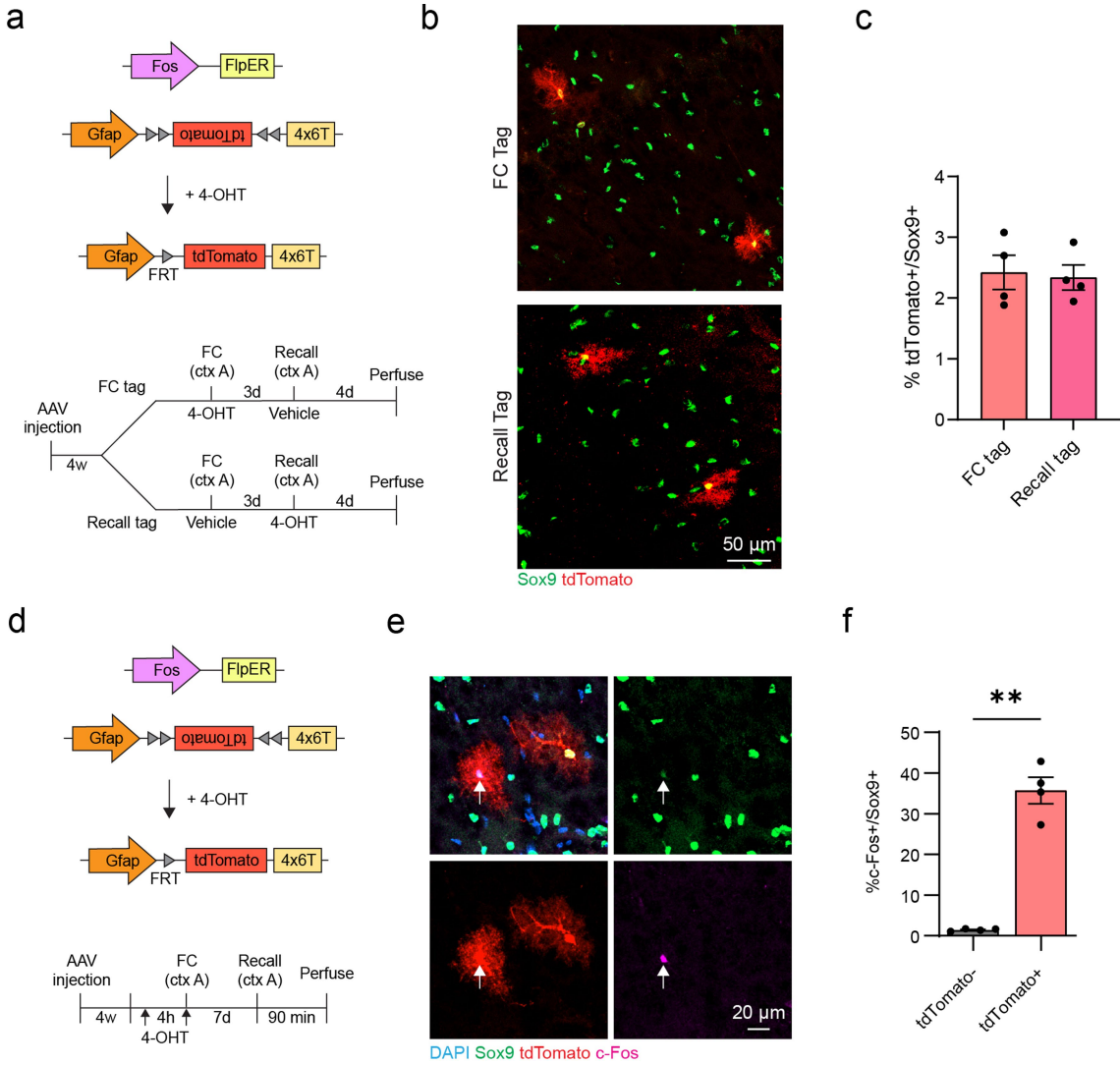
**a.** Timeline for examining astrocytic c-Fos expression after injection of tamoxifen, 4-hydroxytamoxifen, or vehicle. **b.** Representative images of Sox9

and c-Fos immunostaining in CA1 and DG. **c.** Quantification of c-Fos expression in Sox9+ cells. One-way ANOVA,  $P \geq 0.268$ .  $n = 4$  mice per group. Data are mean  $\pm$  SEM.



**Extended Data Fig. 7 | Tagging learning-associated astrocyte ensembles with Fos-FlpER.** **a.** Schematic of genetic system and timeline for evaluating activity-dependent labeling of astrocytes with Fos-FlpER. **b.** Representative images of hippocampal astrocytes labeled in home cage and fear conditioned

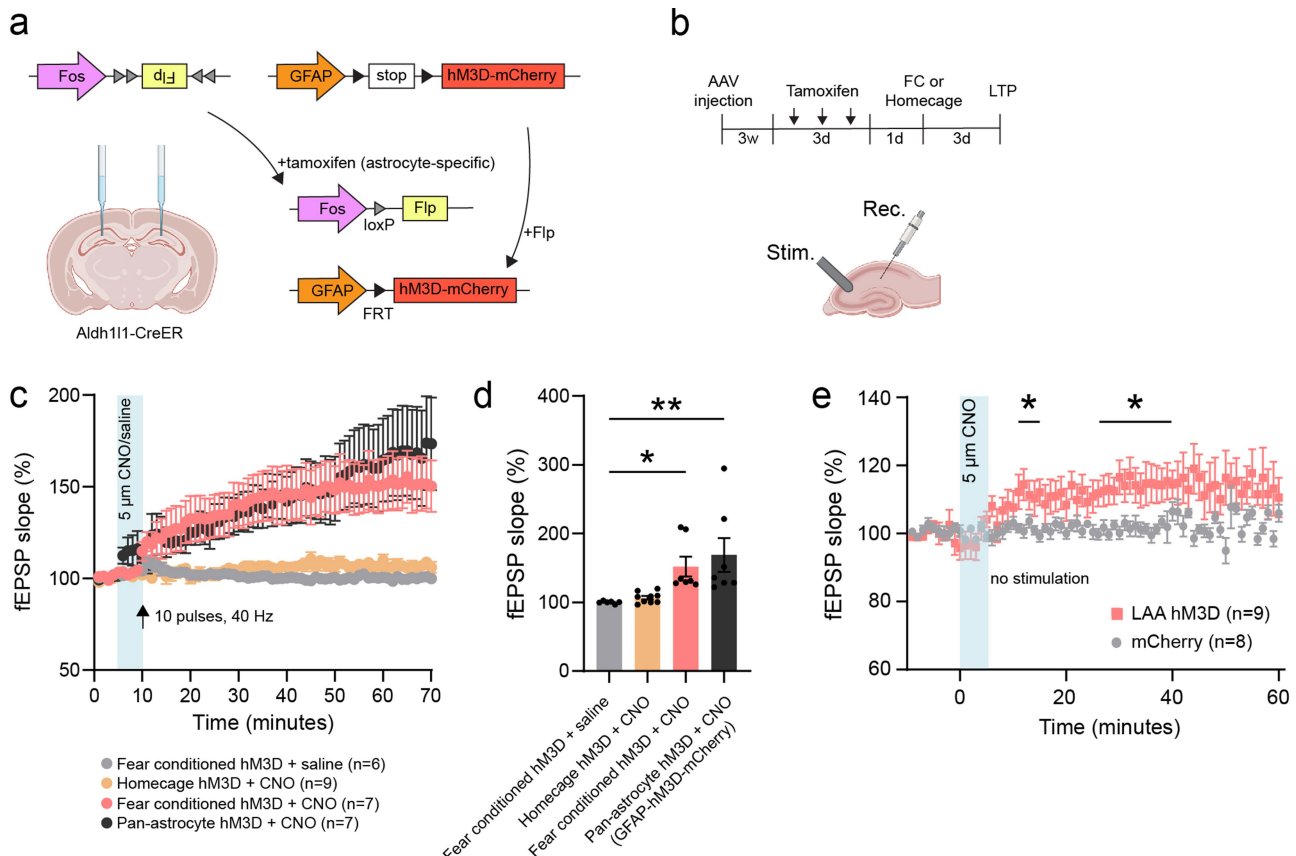
mice. **c.** Quantification of tdTomato<sup>+</sup> cells ( $n = 4$  mice per group, two-tailed t test,  $**P = 0.001$ ). **d.** Representative immunostaining showing colocalization of tdTomato with GFAP. Representative of 4 mice/group. Data are mean  $\pm$  SEM.



**Extended Data Fig. 8 | Learning-associated astrocytes re-express c-Fos after memory recall.** **a.** Schematic of genetic system for labeling learning-associated astrocytes with tdTomato and experimental design for labeling active astrocytes during fear conditioning or recall. **b.** Representative images of tdTomato+ learning associated astrocytes. **c.** Quantification of density of tdTomato+ astrocytes tagged during fear conditioning (FC) or recall ( $N = 4$  mice per group). Two-tailed t test,  $P = 0.818$ . **d.** Schematic of genetic system for labeling learning-associated astrocytes with tdTomato during fear

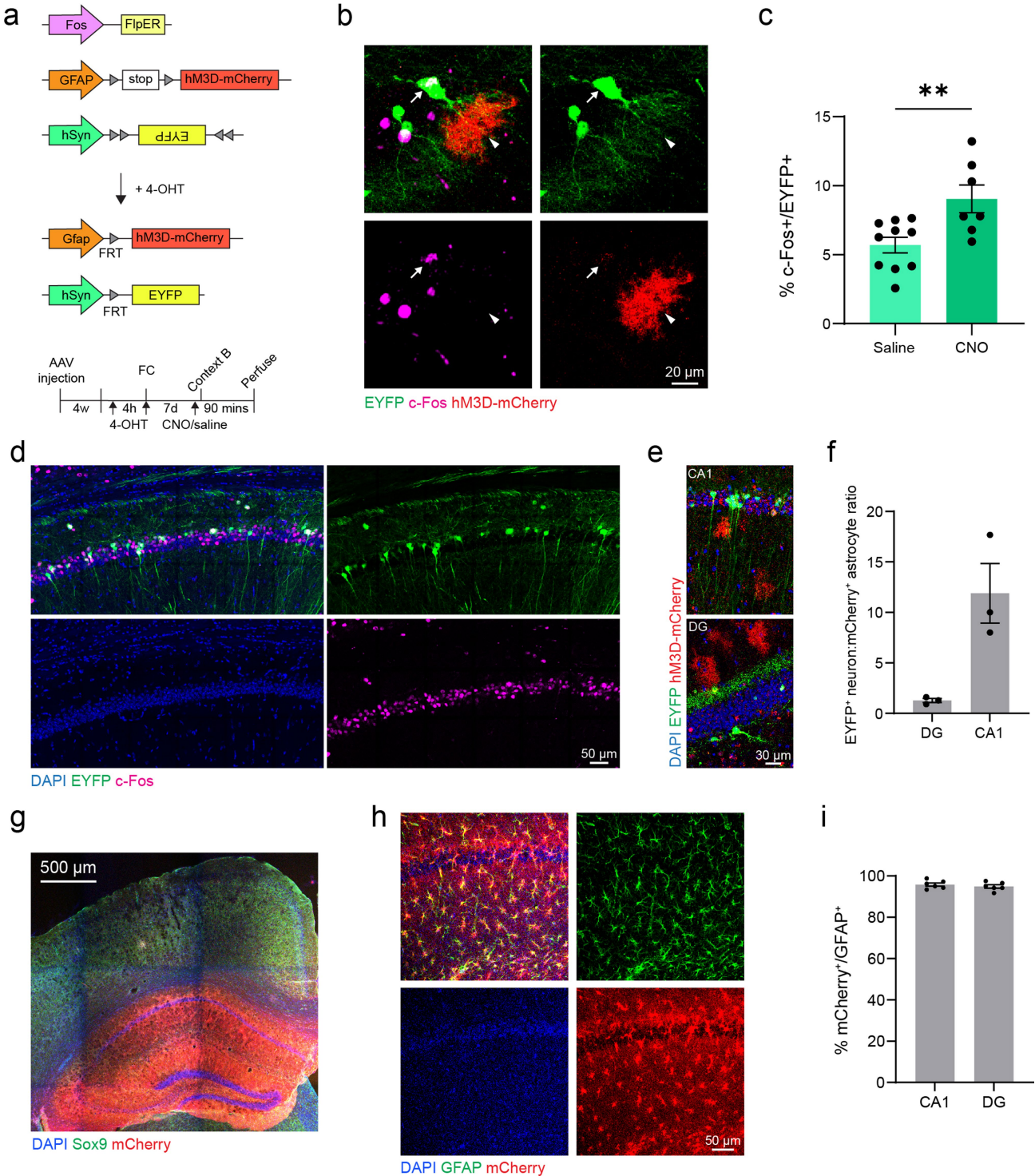
conditioning and experimental design for examining c-Fos expression after memory recall. **e.** Representative image of c-Fos expression in a learning-associated astrocyte after memory recall. Arrow indicates a c-Fos+ tdTomato+ astrocyte. **f.** Quantification of c-Fos expression after recall in Sox9+ non-learning associated astrocytes (tdTomato-) and learning-associated astrocytes following recall (tdTomato+). tdTomato+ astrocytes were ~2.4% of all Sox9+.  $N = 4$  mice, two-tailed Welch's t test,  $**P = 0.002$ . Data are mean  $\pm$  SEM.

# Article



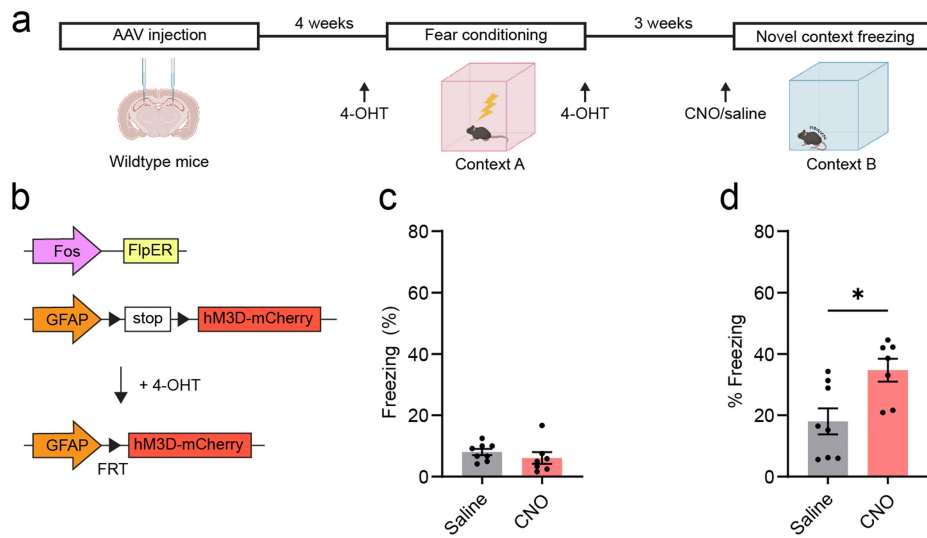
**Extended Data Fig. 9 | Learning-associated astrocytes facilitate long-term potentiation.** **a.** Schematic of genetic system for expressing hM3D-mCherry in learning-associated astrocytes. **b.** Experimental timeline and schematic of LTP recordings. **c.** fEPSP traces from slices treated with CNO or saline followed by subthreshold stimulation (n = 6 fear conditioned hM3D + saline, n = 9 homecage hM3D + CNO, n = 7 fear conditioned hM3D + CNO, n = 7 pan-astrocyte hM3D + CNO mice). **d.** Summary of fEPSP slope from the last 5 min of recordings

in panel c (n = 6 fear conditioned hM3D + saline, n = 9 homecage hM3D + CNO, n = 7 fear conditioned hM3D + CNO, n = 7 pan-astrocyte hM3D + CNO mice). One way ANOVA, P = 0.004; Dunnett's tests, \*P = 0.047, \*\*P = 0.007. **e.** fEPSP traces from slices treated with CNO but without electrical stimulation. Two-tailed t tests comparing 5-minute time bins, \*P ≤ 0.049, n = 9 LAA hM3D and 8 mCherry mice. Data are mean ± SEM. Panel a, b were created using Biorender.com.



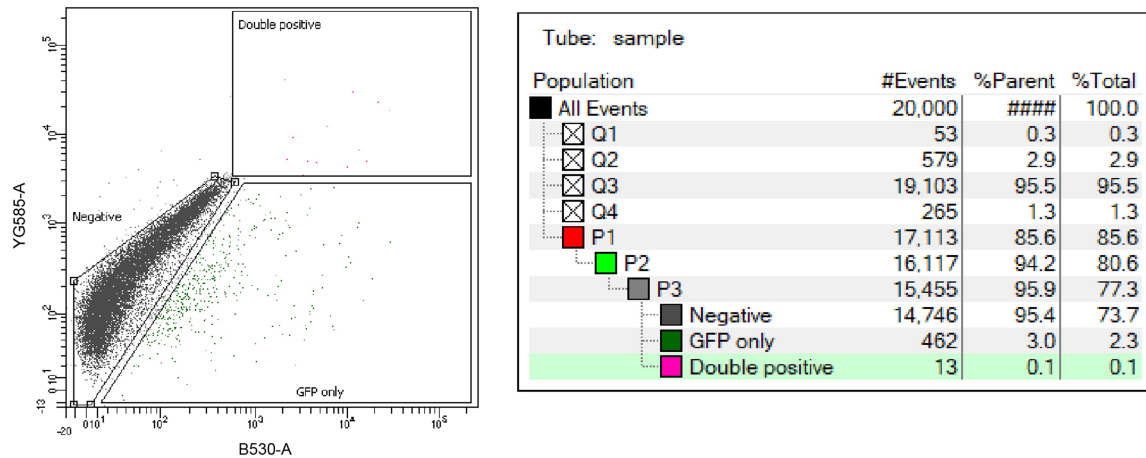
**Extended Data Fig. 10 | Additional characterization of learning-associated astrocyte-engram neuron interactions and viral labeling.** **a.** Schematic of AAVs and experimental timeline related to Fig. 3k–m. **b.** Images showing AAV-mediated labeling and immunostaining for c-Fos in dentate gyrus. Arrow indicates an EYFP+ c-Fos positive engram neuron. Arrowhead indicates an hM3D-mCherry+ astrocyte located within the dendritic arbor of the neuron. The magenta channel fluorescence was subtracted from the red channel in order to offset spectral bleed-through. Representative of 4 mice. **c.** Re-activation of engram neurons in dentate gyrus was increased by learning-associated astrocyte activation (two-tailed t test,  $**P = 0.007$ ).  $n = 10$  saline, 7 CNO mice.

**d.** Low magnification images showing AAV-mediated labeling of engram neurons and immunostaining for c-Fos. **e.** Images of mCherry and EYFP labeled cells in CA1 and DG. Representative of 4 mice. **f.** Quantification of the ratio of engram neurons (EYFP+) to learning-associated astrocytes (mCherry+) in CA1 and DG.  $N = 3$  mice per region. **g.** Low magnification image showing viral targeting of the hippocampus with AAV-GFAP-mCherry. Representative of 8 mice. **h.** Higher magnification image of viral labeling representative of 6 mice. **i.** Quantification of viral labeling of astrocytes.  $n = 6$  mice per region. Data are mean  $\pm$  SEM.

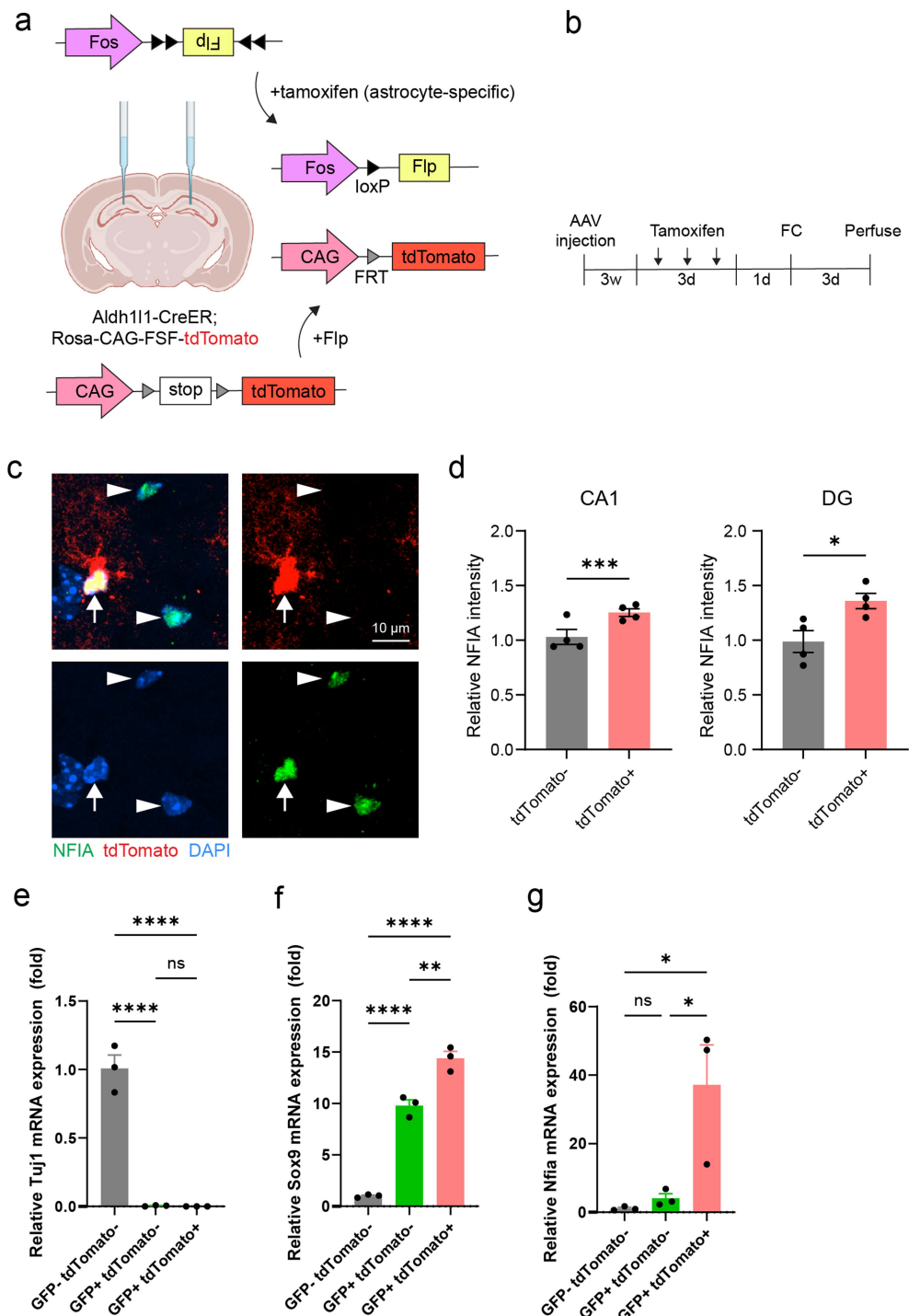


**Extended Data Fig. 11 | Remote reactivation of learning-associated astrocyte ensembles elicits recall. a.** Timeline. **b.** Schematic of genetic system for evaluating recall after remote reactivation of the fear-tagged astrocyte ensemble. **c.** Quantification of freezing behavior prior to foot shocks

(n = 8 saline, n = 7 CNO mice, two-tailed t test, P = 0.368). **d.** Quantification of freezing behavior in a neutral Context B 30 min after injection of 3 mg/kg CNO (n = 8 saline, n = 7 CNO mice, two-tailed t test, \*P = 0.012). Data are mean ± SEM. Panel a was created using Biorender.com.

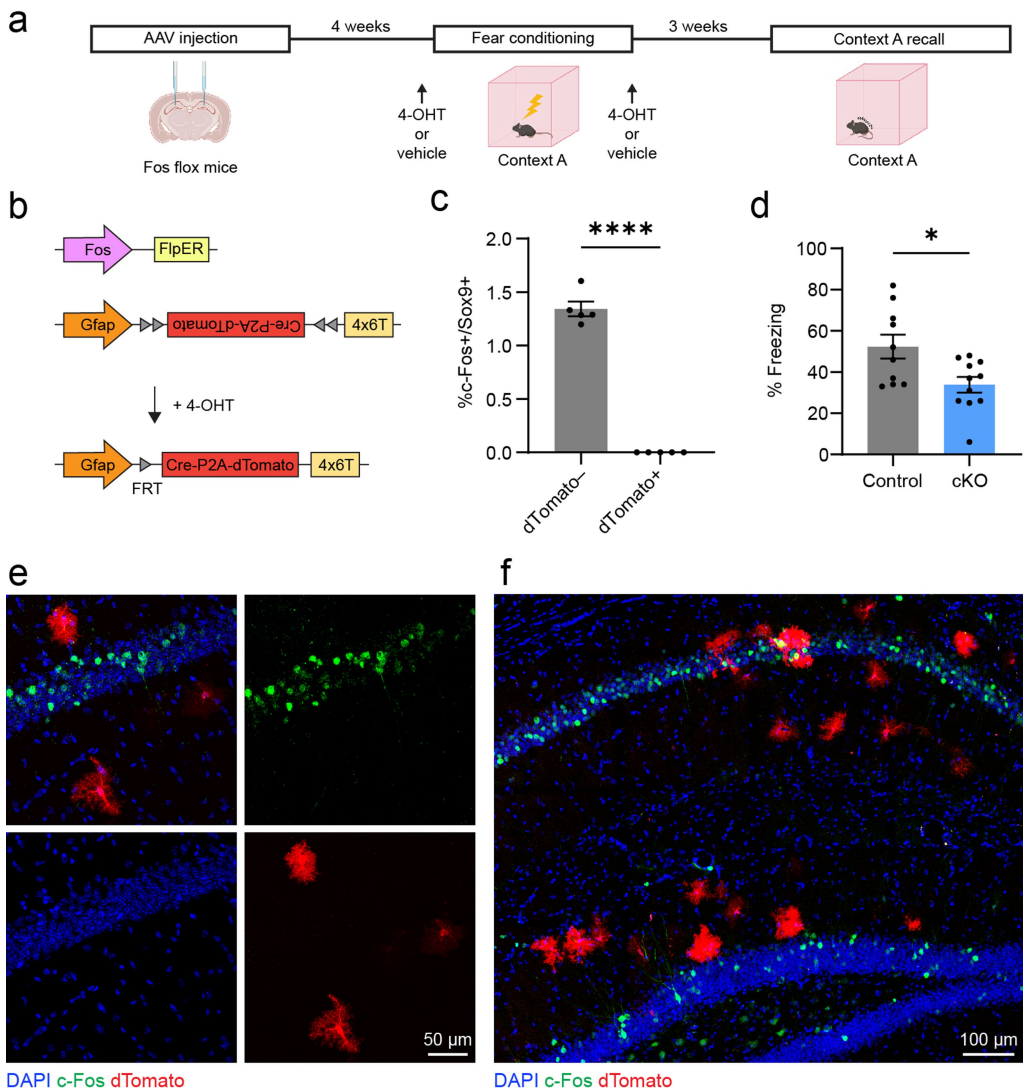


**Extended Data Fig. 12 | Gating strategy for cell sorting.** Example of the gating strategy used for sorting GFP+ tdTomato+ (learning-associated) and GFP+ tdTomato- (non-learning-associated) astrocytes.



**Extended Data Fig. 13 | Validation of increased NFIA in learning-associated astrocytes.** **a.** Schematic of genetic system. **b.** Timeline for labeling learning-associated astrocytes. **c.** Representative immunostaining for NFIA. Arrow indicates tdTomato+ learning-associated astrocyte, arrowheads indicate tdTomato- astrocytes. **d.** Quantification of NFIA fluorescence intensity in tdTomato+ and tdTomato- astrocytes ( $n = 62$  CA1 tdTomato- astrocytes,  $n = 61$  CA1 tdTomato+ astrocytes,  $n = 48$  DG tdTomato- astrocytes,  $n = 52$  tdTomato+ DG astrocytes,  $n = 4$  mice, nested t tests, \* $P = 0.021$ , \*\* $P = 0.001$ ). **e.** RT-qPCR quantification of neuronal Tuj1 mRNA in sorted cell populations. Tuj1 was de-enriched in GFP+ samples ( $n = 3$  technical replicates,  $n = 3$  biological

replicates per group, one-way ANOVA and Tukey's post hoc tests, \*\*\*\* $P < 0.0001$ ). **f.** RT-qPCR quantification of astrocytic Sox9 mRNA in sorted cell populations. Sox9 was enriched in GFP+ samples ( $n = 3$  technical replicates,  $n = 3$  biological replicates per group, one-way ANOVA and Tukey's post hoc tests, \*\* $P = 0.002$ , \*\*\*\* $P < 0.0001$ ). **g.** RT-qPCR quantification of Nfia mRNA in sorted cell populations. Nfia was enriched in GFP+ tdTomato+ samples ( $n = 3$  technical replicates,  $n = 3$  biological replicates per group, one-way ANOVA and Tukey's post hoc tests, \* $P = 0.022$  (top), 0.031 (bottom)). Data are mean  $\pm$  SEM. Panel a was created using Biorender.com.



**Extended Data Fig. 14 | Fos deletion in learning-associated astrocytes impairs memory recall.** **a.** Timeline for Fos knockout in learning-associated astrocytes and examining memory recall. **b.** Schematic of genetic system. **c.** Confirmation of lack of Fos expression in dTomato+ learning-associated astrocytes relative to dTomato- astrocytes (N = 5 mice, two-tailed Welch's t test, \*\*\*\*P < 0.0001). **d.** Quantification of freezing behavior during recall test in

Context A. N = 10 Control (vehicle injected), N = 11 Fos cKO mice; two-tailed t test, \*P = 0.014. **e.** Representative image showing lack of c-Fos expression in dTomato+ astrocytes. Representative of 5 mice. **f.** Low magnification image of learning-associated astrocyte labeling in CA1 and DG. Note that no dTomato+ astrocytes express c-Fos. Representative of 5 mice. Panel a was created using Biorender.com.

## Reporting Summary

Nature Portfolio wishes to improve the reproducibility of the work that we publish. This form provides structure for consistency and transparency in reporting. For further information on Nature Portfolio policies, see our [Editorial Policies](#) and the [Editorial Policy Checklist](#).

### Statistics

For all statistical analyses, confirm that the following items are present in the figure legend, table legend, main text, or Methods section.

n/a Confirmed

- The exact sample size ( $n$ ) for each experimental group/condition, given as a discrete number and unit of measurement
- A statement on whether measurements were taken from distinct samples or whether the same sample was measured repeatedly
- The statistical test(s) used AND whether they are one- or two-sided  
*Only common tests should be described solely by name; describe more complex techniques in the Methods section.*
- A description of all covariates tested
- A description of any assumptions or corrections, such as tests of normality and adjustment for multiple comparisons
- A full description of the statistical parameters including central tendency (e.g. means) or other basic estimates (e.g. regression coefficient) AND variation (e.g. standard deviation) or associated estimates of uncertainty (e.g. confidence intervals)
- For null hypothesis testing, the test statistic (e.g.  $F$ ,  $t$ ,  $r$ ) with confidence intervals, effect sizes, degrees of freedom and  $P$  value noted  
*Give  $P$  values as exact values whenever suitable.*
- For Bayesian analysis, information on the choice of priors and Markov chain Monte Carlo settings
- For hierarchical and complex designs, identification of the appropriate level for tests and full reporting of outcomes
- Estimates of effect sizes (e.g. Cohen's  $d$ , Pearson's  $r$ ), indicating how they were calculated

*Our web collection on [statistics for biologists](#) contains articles on many of the points above.*

### Software and code

Policy information about [availability of computer code](#)

#### Data collection

Confocal imaging was conducted with Zeiss LSM 880 laser scanning confocal microscope and Zen software (v3.1). Calcium imaging: GECIquant (v1.0), ImageJ (v1.54f), and Clampfit (v10.7) were used to analyze calcium signals. FACS-sorting was performed using a Becton Dickinson FACStar II with FACSDiva software. RNA-seq was performed on Illumina Nextseq system suite. Images in schematics were created using Biorender.com.

#### Data analysis

ImageJ (v1.54f) was used for confocal image analysis. Clampfit (10.7) was used for electrophysiological data analysis. The following were used for calcium image analysis: GECIquant, ImageJ (v1.54f), Clampfit (10.7). The following were used for RNA-seq and bioinformatic analyses: RNA-seq data was processed using fastQC (v0.11.7), MultiQC (v1.6), STAR (v2.5.0a), HOMER (v4.10), and DESeq2 (v1.30.1). Graphpad Prism (v10) was used for all statistical analysis.

For manuscripts utilizing custom algorithms or software that are central to the research but not yet described in published literature, software must be made available to editors and reviewers. We strongly encourage code deposition in a community repository (e.g. GitHub). See the Nature Portfolio [guidelines for submitting code & software](#) for further information.

## Data

Policy information about [availability of data](#)

All manuscripts must include a [data availability statement](#). This statement should provide the following information, where applicable:

- Accession codes, unique identifiers, or web links for publicly available datasets
- A description of any restrictions on data availability
- For clinical datasets or third party data, please ensure that the statement adheres to our [policy](#)

The RNA-seq data are available at GEO with accession ID GSE254016. The analyzed RNA-seq data are provided as Extended data Excel file 1.

## Research involving human participants, their data, or biological material

Policy information about studies with [human participants or human data](#). See also policy information about [sex, gender \(identity/presentation\), and sexual orientation](#) and [race, ethnicity and racism](#).

Reporting on sex and gender

N/A

Reporting on race, ethnicity, or other socially relevant groupings

N/A

Population characteristics

N/A

Recruitment

N/A

Ethics oversight

N/A

Note that full information on the approval of the study protocol must also be provided in the manuscript.

## Field-specific reporting

Please select the one below that is the best fit for your research. If you are not sure, read the appropriate sections before making your selection.

Life sciences

Behavioural & social sciences

Ecological, evolutionary & environmental sciences

For a reference copy of the document with all sections, see [nature.com/documents/nr-reporting-summary-flat.pdf](https://nature.com/documents/nr-reporting-summary-flat.pdf)

## Life sciences study design

All studies must disclose on these points even when the disclosure is negative.

Sample size

No formal estimates of statistical power were done. Sample sizes were based on previous publications using similar techniques. Animal numbers were minimized to conform to ethical guidelines while maintaining adequate numbers to derive accurate measurements.

Data exclusions

There were no data exclusions.

Replication

All attempts at replication were successful. Mice from multiple litters were used to attain at least 3 biological replicates per group for each measurement.

Randomization

Mice were randomly allocated to groups when possible. Where dependent on genotype, mice from multiple litters were randomly selected to be used.

Blinding

Investigators were blinded to group allocation during experimentation and data analysis.

## Reporting for specific materials, systems and methods

We require information from authors about some types of materials, experimental systems and methods used in many studies. Here, indicate whether each material, system or method listed is relevant to your study. If you are not sure if a list item applies to your research, read the appropriate section before selecting a response.

## Materials & experimental systems

n/a	Involved in the study
<input type="checkbox"/>	<input checked="" type="checkbox"/> Antibodies
<input checked="" type="checkbox"/>	<input type="checkbox"/> Eukaryotic cell lines
<input checked="" type="checkbox"/>	<input type="checkbox"/> Palaeontology and archaeology
<input type="checkbox"/>	<input checked="" type="checkbox"/> Animals and other organisms
<input checked="" type="checkbox"/>	<input type="checkbox"/> Clinical data
<input checked="" type="checkbox"/>	<input type="checkbox"/> Dual use research of concern
<input checked="" type="checkbox"/>	<input type="checkbox"/> Plants

## Methods

n/a	Involved in the study
<input checked="" type="checkbox"/>	<input type="checkbox"/> ChIP-seq
<input type="checkbox"/>	<input checked="" type="checkbox"/> Flow cytometry
<input checked="" type="checkbox"/>	<input type="checkbox"/> MRI-based neuroimaging

## Antibodies

### Antibodies used

The following primary antibodies were used: rat anti-c-Fos (1:5000; Synaptic Systems, 226 017), guinea pig anti-Cre (1:1000; Synaptic Systems, 257 004), chicken anti-GFAP (1:1000; abcam, ab4674), rabbit anti-GFAP (1:1000; DAKO, Z0334), rabbit anti-HA (1:500; Roche, 11867423001), rabbit anti-NeuN (1:2000, Millipore, MABN140), rabbit anti-NFIA (1:500; Sigma, HPA006111), rabbit anti-RFP (1:500; Rockland, 600-401-379), and rabbit anti-Sox9 (1:500; Millipore, AB5535). The following secondary antibodies were used: Alexa Fluor 488-conjugated donkey anti-chicken (1:500; Jackson ImmunoResearch, 703-545-155), Alexa Fluor 647-conjugated donkey anti-chicken (1:500; Jackson ImmunoResearch, 703-605-155), Alexa Fluor 594-conjugated donkey anti-guinea pig (1:500; Jackson ImmunoResearch, 706-585-148), Alexa Fluor 488-conjugated donkey anti-rabbit (1:500; Jackson ImmunoResearch, 711-545-152), Alexa Fluor 594-conjugated donkey anti-rabbit (1:500; Jackson ImmunoResearch, 711-605-152), Alexa Fluor 647-conjugated donkey anti-rabbit (1:500; Jackson ImmunoResearch, 712-545-153), Alexa Fluor 594-conjugated donkey anti-rat (1:500; Jackson ImmunoResearch, 712-585-153), Alexa Fluor 647-conjugated donkey anti-rat (1:500; Jackson ImmunoResearch, 712-605-153).

### Validation

Antibodies were validated by manufacturers and used in previously published work. Appropriate primary antibody dilutions were determined by testing multiple dilutions on sample mouse brain tissue. Secondary antibody only controls were used to confirm lack of signal in the absence of primary antibodies.

Rat anti-c-Fos Synaptic Systems 226 017: Manufacturer states this is a monoclonal antibody validated for use in immunostaining mouse tissue. Clone number 108B5H5. Immunogen is a synthetic peptide corresponding to residues near the amino terminus of rat c-Fos (UniProt Id: P12841). Previously used in PMID: 36289226.

Guinea pig anti-Cre recombinase Synaptic Systems 257 004: Manufacturer states this is a polyclonal antibody validated for use in immunostaining mouse tissue. Immunogen is full length recombinant Cre-recombinase from Bacteriophage P1 (UniProt Id: P06956). Previously used in PMID: 32991831.

Chicken polyclonal anti-GFAP Abcam ab4674: Manufacturer states immunogen is recombinant full length protein corresponding to Human GFAP. Isotype 1 expressed in and purified from *E. coli*. Validated for immunohistochemistry in mouse brain tissue. Used in PMID: 37393623.

Rabbit polyclonal anti-GFAP Dako Z0334: Manufacturer states immunogen is GFAP isolated from cow spinal cord. The antibody has been solid-phase absorbed with human and cow serum proteins. In crossed immunoelectrophoresis using 50 µL antibody per cm<sup>2</sup> gel area, no reaction with 2 µL human plasma and 2 µL cow serum is observed. The antibody shows one distinct precipitate (GFAP) with cow brain extract. GFAP shows 90-95% homology between species, and, as demonstrated by immunohistochemistry, the antibody reacts strongly with human GFAP. Used for immunohistochemistry in mouse brain tissue in PMID: 33910014.

Rabbit anti-HA Roche 11867423001: Manufacturer states this antibody is a monoclonal antibody to the HA-peptide (clone 3F10). Recognizes the HA peptide sequence (YPYDVPDYA), derived from the influenza hemagglutinin protein (immunogen is amino acids 98-106). Validated for use in immunocytochemistry.

Rabbit monoclonal anti-NeuN Millipore MABN140: Manufacturer states validated for use in immunohistochemistry in mouse brain tissue. Used in PMID: 35177618.

rabbit anti-NFIA Sigma HPA006111: Sequence of immunogen: LKSVEDEMDSPGEEPFYTQQGRSPGSGQSSGWHEVEPGMPSPTTLKSEKSGFSSPSQTSSLGTAFTQHHRPVITGPRASPHATPSTLHFPTSPIQQ. Validated for use in immunohistochemistry. Previously used in PMID: 32320644.

Rabbit anti-RFP Rockland 600-401-379: Manufacturer states the immunogen is a Red Fluorescent Protein fusion protein corresponding to the full-length amino acid sequence (234aa) derived from the mushroom anemone *Discosoma*. This product was prepared from monospecific antiserum by immunoaffinity chromatography using Red Fluorescent Protein (*Discosoma*) coupled to agarose beads followed by solid phase adsorption(s) to remove any unwanted reactivities. Validated for immunostaining.

Rabbit anti-Sox9 Millipore AB5535: Manufacturer states the immunogen is a KLH-conjugated linear peptide corresponding to the C-terminal sequence of human Sox9. Validated for use in immunohistochemistry. Previously used in PMID: 32320644.

All secondary antibodies (Jackson Immunoresearch) were purified from antisera by immunoaffinity chromatography using antigens coupled to agarose beads. These antibodies display minimal cross reactivity to off-target species.

## Animals and other research organisms

Policy information about [studies involving animals](#); [ARRIVE guidelines](#) recommended for reporting animal research, and [Sex and Gender in Research](#)

### Laboratory animals

The following transgenic mouse strains were used: Fos-flox (037115-JAX), Rosa-CAG-LSL-tdTomato (Ai14; Jackson Laboratory, 007914), Rosa-CAG-FSF-tdTomato (Ai65F; Jackson Laboratory, 032864), Aldh1l1-CreER (Jackson Laboratory, 029655), Aldh1l1-GFP (RRID:MMRRC\_011015-UCD), and NFIA-flox. All mice were on a C57/b6 background.

Wild animals	No wild animals were used in this study.
Reporting on sex	Mice of both sexes were used. Data was not stratified nor analyzed based on sex.
Field-collected samples	No field-collected samples were used.
Ethics oversight	Experiments were conducted in accordance with protocols approved by the Institutional Animal Care and Use Committee at Baylor College of Medicine.

Note that full information on the approval of the study protocol must also be provided in the manuscript.

## Plants

Seed stocks	N/A
Novel plant genotypes	N/A
Authentication	N/A

## Flow Cytometry

### Plots

Confirm that:

- The axis labels state the marker and fluorochrome used (e.g. CD4-FITC).
- The axis scales are clearly visible. Include numbers along axes only for bottom left plot of group (a 'group' is an analysis of identical markers).
- All plots are contour plots with outliers or pseudocolor plots.
- A numerical value for number of cells or percentage (with statistics) is provided.

### Methodology

Sample preparation	Mice were perfused with cold saline and hippocampi were dissected on ice. Dissected tissue was dissociated as previously described (PMID: 28166219).
Instrument	BD FACSAria II
Software	BD FACSDiva software
Cell population abundance	Enrichment of astrocytes and de-enrichement of neurons were confirmed by qPCR of cDNA libraries prepared from sorted samples.
Gating strategy	Singlet gating was done based on forward and side scatter. Singlet events were assessed for GFP and tdTomato fluorescence. Non-fluorescent brain tissue was used as a negative control to set the double negative population gate. We also performed single color controls to establish ideal voltage, potential compensation, and gating. The GFP signal was detected with a 488nm laser, through a 505nm long pass filter, and 530/30 detector. tdTomato signal was detected with 561nm laser, through a 570 long pass filter, and 585/51 detector.

Tick this box to confirm that a figure exemplifying the gating strategy is provided in the Supplementary Information.